

**The glacial and Holocene history of Notre Dame Trough, Northeast  
Newfoundland Shelf**

By  
Logan Robertson

A Thesis Submitted to  
Saint Mary's University, Halifax Nova Scotia  
In Partial Fulfillment of the Requirements for a  
Bachelor of Science Honours Degree in Geology

April 2018, Halifax, Nova Scotia

Copyright Logan S. Robertson, 2018

Approved: Dr. David Piper  
External supervisor

Approved: Dr. Georgia Pe-Piper  
Internal supervisor

Date: April 12, 2018

# **The glacial and Holocene history of Notre Dame Trough, Northeast Newfoundland Shelf**

By Logan Robertson

Date: April 12th

## **Abstract**

This study was conducted on the Notre Dame Trough (NDT) on the Northeast Newfoundland Shelf. The purpose of this project was to help unravel the glacial history, including the timing of a large slide block in the NDT, and to compare the late Quaternary sedimentary record in cores with other places on the Newfoundland margin. Air gun seismic and Olex bathymetry were used to determine that some features present in the NDT are glaciotectonic in origin, and likely formed during the Wisconsinan. A large slide block present in the NDT was analyzed using seismic survey data and down-core shear strength data and showed that this slide block likely post-dates the glaciotectonic deformation.

The physical properties of thirteen piston cores and chemical properties of five of the cores were analyzed to classify four main sediment units. Knudsen 3.5 kHz seismic data were used to determine the sedimentary context of the cores. Carbon-14 dates from these cores provide age control for changes in sediment supply and paleoceanographic events such as Heinrich events with high supply of detrital carbonate.

The variation in sediment source in the study area indicates that the NDT was largely unaffected by the Labrador current for some time before 14 ka. Correlations between the cores of this study and those of Flemish Pass and Cartwright Saddle have compared the paleoceanographic records and show that Heinrich-0 (ca. 12 ka) can be correlated between NDT, Flemish Pass and Cartwright Saddle. However, based on Carbon-14 dates, Heinrich-1 is not marked by a detrital carbonate layer in Notre Dame Trough. A red mud bed correlated between several cores may represent a synchronous meltwater discharge event from ice in St Anthony Basin.

## **Acknowledgements**

I would like to thank my supervisor Georgia Pe-Piper and my external supervisor David Piper. They gave me the opportunity undertake this honours project at Saint Mary's University. I would like to extend an extra thank you to David Piper for mentoring me as a geoscientist. Thank you for providing edits and advice during the process of writing this honours thesis.

I would also like to thank the Geological Survey of Canada for allowing me to take on a project affiliated with them and the staff at the Bedford Institute of Oceanography. Specifically, I would like to thank Calvin Campbell and Kate Jarrett. They gave me access for helping me in obtaining data using their computer software.

## Table of Contents

1 INTRODUCTION .....	1
2 GEOLOGICAL SETTING AND HISTORY .....	1
2.1 OCEANOGRAPHIC SETTING.....	3
2.2 REGIONAL GEOLOGY .....	5
2.3 BATHYMETRY.....	6
2.4 GLACIAL HISTORY.....	7
2.5 DEGLACIAL HISTORY .....	8
2.6 HOLOCENE.....	9
3 MATERIALS & METHODS .....	10
3.1 SHIPBOARD ACTIVITY .....	10
3.2 LOCATION OF CORES .....	10
3.3 GEOMORPHOLOGY .....	12
3.4 SEISMIC.....	13
3.5 CORE DESCRIPTION.....	13
3.6 PORTABLE X-RAY FLUORESCENCE (PXRF).....	13
3.7 SPECTROPHOTOMETRY .....	14
3.8 RAW DATA .....	15
4 RESULTS .....	15
4.1 MORPHOLOGY .....	15
4.2 SEISMIC REFLECTORS.....	17
4.2.1 GI GUN.....	17
4.2.2 SEISMIC FACIES .....	22
4.2.3 SEISMIC UNITS .....	24
4.2.4 KNUDSEN 3.5 KHZ PROFILES .....	24
4.3 LITHOSTRATIGRAPHY .....	26
4.3.1 INTRODUCTION .....	26
4.3.2 CORE DESCRIPTIONS.....	26
4.3.3 SUMMARY OF LITHOSTRATIGRAPHY .....	39
4.4 GEOCHEMISTRY OF CORES .....	39

4.4.1 PORTABLE X-RAY FLUORESCENCE (PXRF) SUMMARY .....	39
4.4.2 PROVENANCE.....	45
4.5 COLOUR .....	52
4.5.1 LIGHTNESS L* .....	52
4.5.2 REDNESS A* .....	53
4.6 C-14 DATING .....	53
5. DISCUSSION .....	54
5.1 INTERPRETATION OF SEISMIC UNITS AND FACIES .....	54
5.2 GLACIOTECTONICS .....	56
5.3 CORRELATION OF CORES AND AGE MODEL .....	61
5.4 PRE-DEGLACIAL HISTORY.....	64
5.5 DEGLACIAL HISTORY .....	65
5.6 THE ROLE OF THE LABRADOR CURRENT.....	67
5.7 RELATIVE AGE OF THE SLIDE.....	69
6. RECOMMENDED WORK .....	70
6.1 CARBON DATING.....	70
7 CONCLUSIONS.....	70
REFERENCES .....	72
WEB REFERENCES.....	74

## List of Figures

Figure 1 – Locality map.....	2
Figure 2 – Map of ocean currents .....	4
Figure 3 – Bedrock map.....	5
Figure 4 – Olex data interpretation .....	7
Figure 5 – Map of seismic profiles and core localities .....	12
Figure 6 – Map of geomorphology .....	16
Figure 7 – GI gun seismic profile showing Notre Dame Unconformity .....	18
Figure 8 – Seismic profile showing the Middle Mound .....	19
Figure 9 – Seismic profile of the shelf break .....	20
Figure 10 – Seismic profile at the base of the continental slope.....	21
Figure 11 – Seismic facies .....	23
Figure 12 – Seismic units.....	24
Figure 13 – 3.5 kHz seismic profile.....	25
Figure 14a – Core plot legend.....	34
Figure 14b – Downcore summary of cores 1, 2, 3, and 4 .....	35
Figure 14c – Downcore summary of cores 5, 6, 7, and 13 .....	36
Figure 14d – Downcore summary of cores 8 and 9 .....	37
Figure 14e – Downcore summary of cores 10, 11, and 12 .....	38
Figure 15a – Downcore XRF of core 2.....	40
Figure 15b – Downcore XRF of core 3. ....	41
Figure 15c – Downcore XRF of core 8.....	42
Figure 15d – Downcore XRF of core 11. ....	43
Figure 15e – Downcore XRF of core 12.....	44
Figure 16a – Rb vs K <sub>2</sub> O for cores 2 and 11. ....	46
Figure 16b – Rb vs K <sub>2</sub> O for core 12. ....	47
Figure 17a – Zr vs Ti plots for cores 2 and 11.....	49
Figure 17b – Zr vs Ti for core 12.....	50
Figure 18a – Sr vs Ca for cores 2 and 11.....	51
Figure 18b – Sr vs Ca for cores 2 and 11.....	52

Figure 19 – Seismic unit summary .....	55
Figure 20 – Seismic profiles showing glide planes.....	58
Figure 21 – Seismic profile of berms.....	60
Figure 22 – Glaciotectonism of the Middle Mound.....	61
Figure 23 – Correlation with Cartwright Saddle and Flemish Pass.....	63
Figure 24 – Fresh water outwash .....	66

## List of Tables

Table 1 – Core localities and water depths .....	11
Table 2 – Carbon-14 dates .....	54

## **1 Introduction**

The Notre Dame Trough (NDT) is a major glacial erosion feature on the Northeast Newfoundland Shelf. Shaw et al. (2011) interpreted the complex bathymetry in the central part of NDT as resulting from glaciotectonic deformation and a young sediment slide. In 2010, 3.5 kHz and airgun seismic profiles and piston cores were collected from the glaciotectonic and slide features to test the hypotheses of Shaw et al. (2011). The piston core data were not worked up in detail at that time. Two long piston cores (6 and 11) were intended to provide chronology of the basin fill, in the hope that it could be traced laterally into at least the slide. Shaw and Longva (2017) proposed a bathymetric based interpretation of the glacial history of NDT, suggesting that it is largely formed by glaciotectonism.

There are three objectives of this study. (1) Confirm or modify the glacial history and glaciotectonic interpretation of Shaw and Longva (2017), based on the new airgun interpretation. (2) Interpret the location, style and age of the slide block in the study area. (3) Interpret the post-glacial (Holocene) palaeoceanographic record of the Labrador Current and compare it with Flemish Pass and Cartwright Saddle.

## **2 Geological setting and history**

The Northeast Newfoundland shelf is a wide margin of continental shelf offshore from the island of Newfoundland. The Notre Dame Channel extends across the Northeast Newfoundland shelf seaward into the Notre Dame Trough (Shaw et al., 2011). The study area is the Notre Dame Trough, which is located north-east of Newfoundland on the Continental Shelf (Fig. 1). The NDT is ~200 km off the coast of Newfoundland. The

trough is over 100 kilometres long and 30 kilometres wide. In the NDT there is a northern basin and a southern basin, which are separated by a large mound of sediment. As pointed out by Shaw et al. (2011), in Notre Dame Trough there are berms along the ridges and within basins. On the western side of the trough there is a block that has undergone sliding (Shaw et al., 2011).

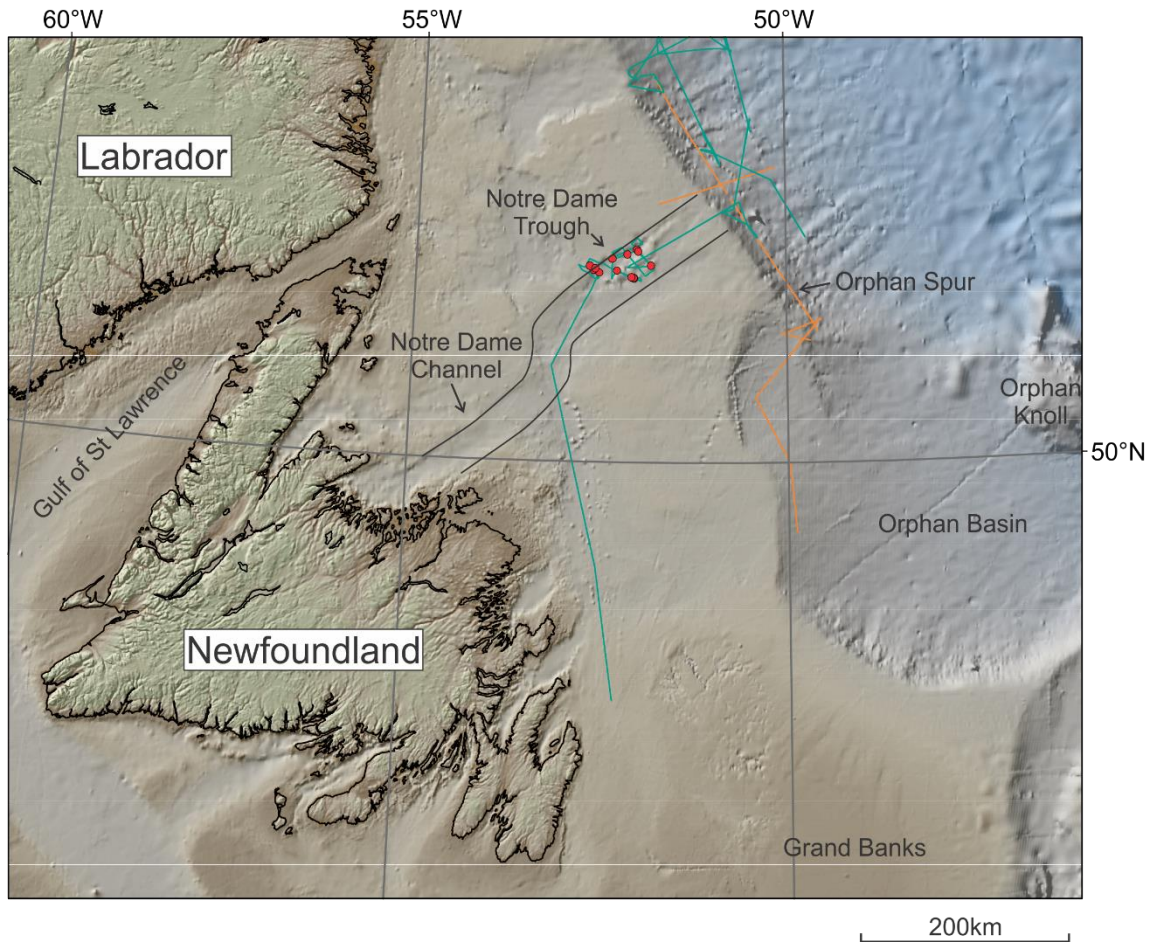


Figure 1. The Notre Dame Trough on the Labrador shelf in relation to Newfoundland and Labrador. The blue lines indicate the ships track during the Hudson expedition 2010-023, some of these correspond to air-gun seismic profiles. The orange lines indicate seismic profiles, which were taken during previous expeditions. The red dots indicate core locations in the study area.

## **2.1 Oceanographic setting**

The Notre Dame Trough is strongly affected by the Labrador Current (Fig. 2). The Labrador Current is sourced from the Arctic Ocean and moves south along the eastern continental margin of Canada (Lazier & Wright, 1993). As the current would have carried ice calved from past glaciers, it would likely be a major contributor to any ice rafted detritus found within cores taken from Notre Dame Trough. Ice streams proposed by Shaw and Longva (2017) suggest that a large source of sediment and ice-rafted detritus (IRD) would be sourced from southern Labrador, the Great Northern Peninsula of Newfoundland and Notre Dame Bay.

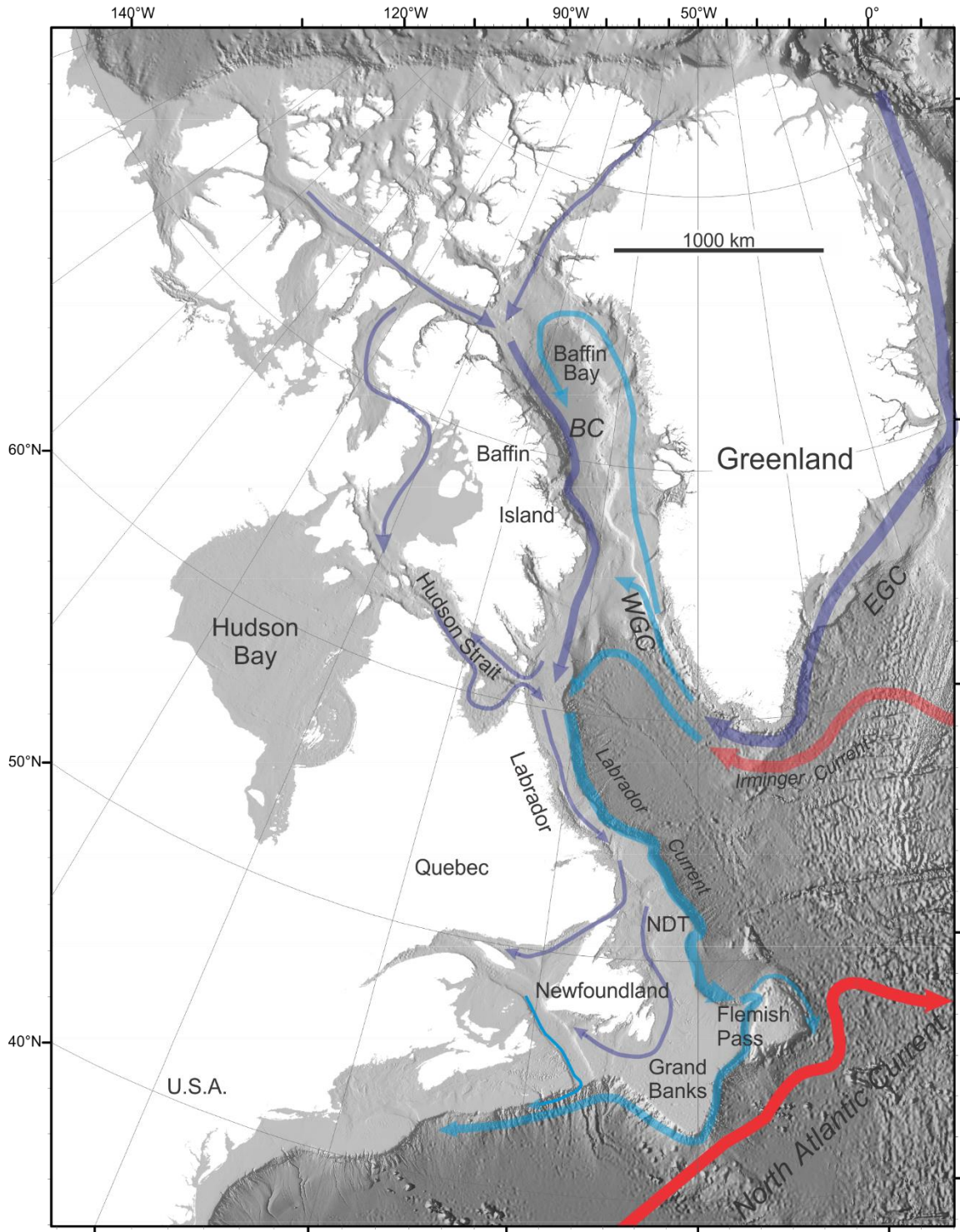


Figure 2. Ocean currents present along the eastern Canadian coast. This shows the main source of water is from the Labrador Current and Hudson Strait. Modified from Rashid et al. (2017). The red lines show warm currents and the light and dark blue lines show cold currents.

## 2.2 Regional geology

The outer shelf overlies sedimentary rock of Mesozoic to Cenozoic age (Shaw et al. 2011). Beneath the inner shelf is the St Anthony Basin, which is a Carboniferous sedimentary basin that largely consists of red beds (Fig. 3). The St Anthony Basin overlies Precambrian/Paleozoic basement and on its eastern side Mesozoic-Cenozoic sediments overlie it (Keen and Williams, 1990, page 157).

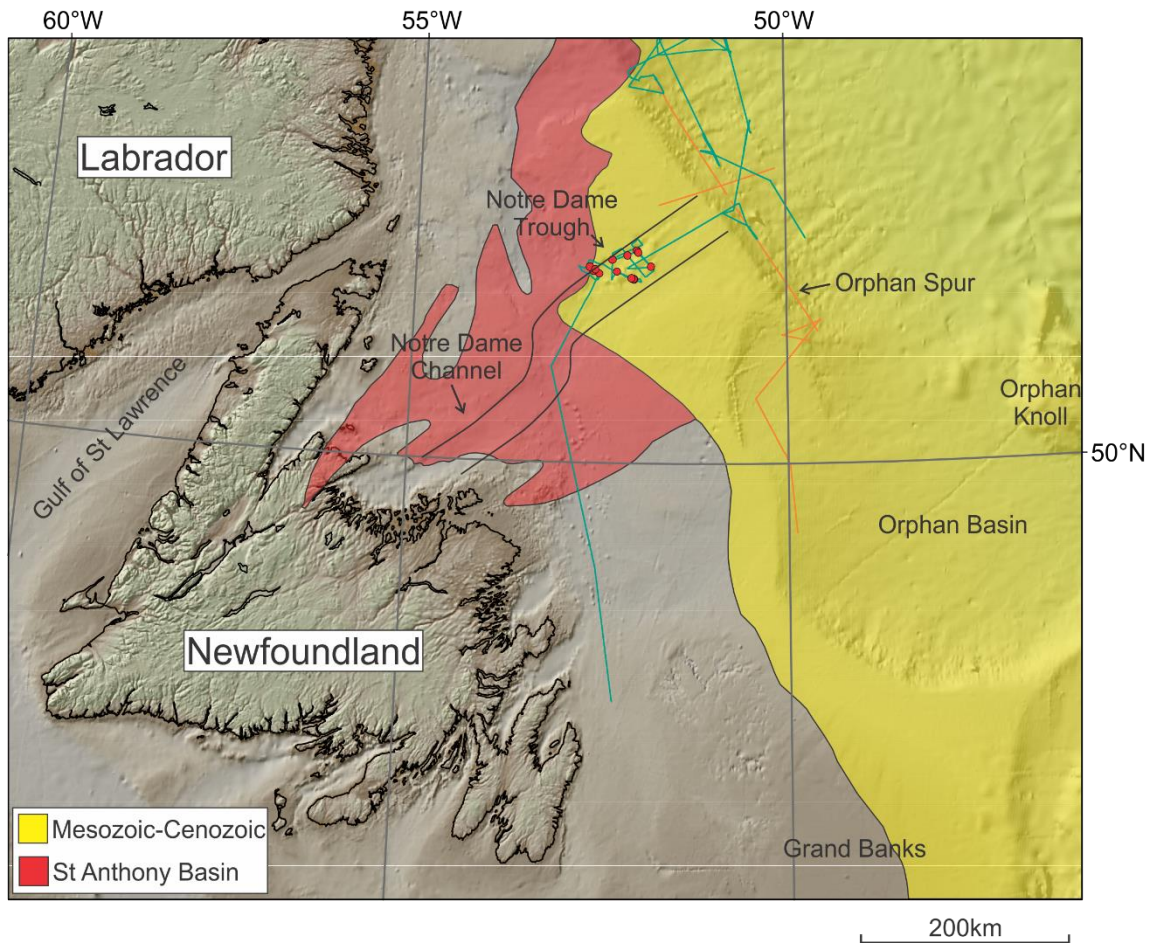


Figure 3. Map showing distribution of bedrock on the North East Newfoundland Shelf.

### **2.3 Bathymetry**

Shaw et al. (2011) have a bathymetric interpretation of Notre Dame Trough using Olex imagery ([http://www.olex.no/index\\_e.html](http://www.olex.no/index_e.html)) of the Northeast Newfoundland Shelf. They proposed two mechanisms for their observations: (1) submarine sliding and (2) glaciotectonism. Figure 4, modified from Shaw et al (2011), shows interpreted glaciotectonism and sliding. The features 'a' and 'b' are interpreted to be caused by glaciotectonics resulting in the movement of Quaternary sediment. Shaw et al (2011) also pointed out how the shallow gradients of the glaciotectonic features suggests against sliding. The features labeled 'c' and 'd' are interpreted to have been caused by sliding (Shaw et al., 2011).

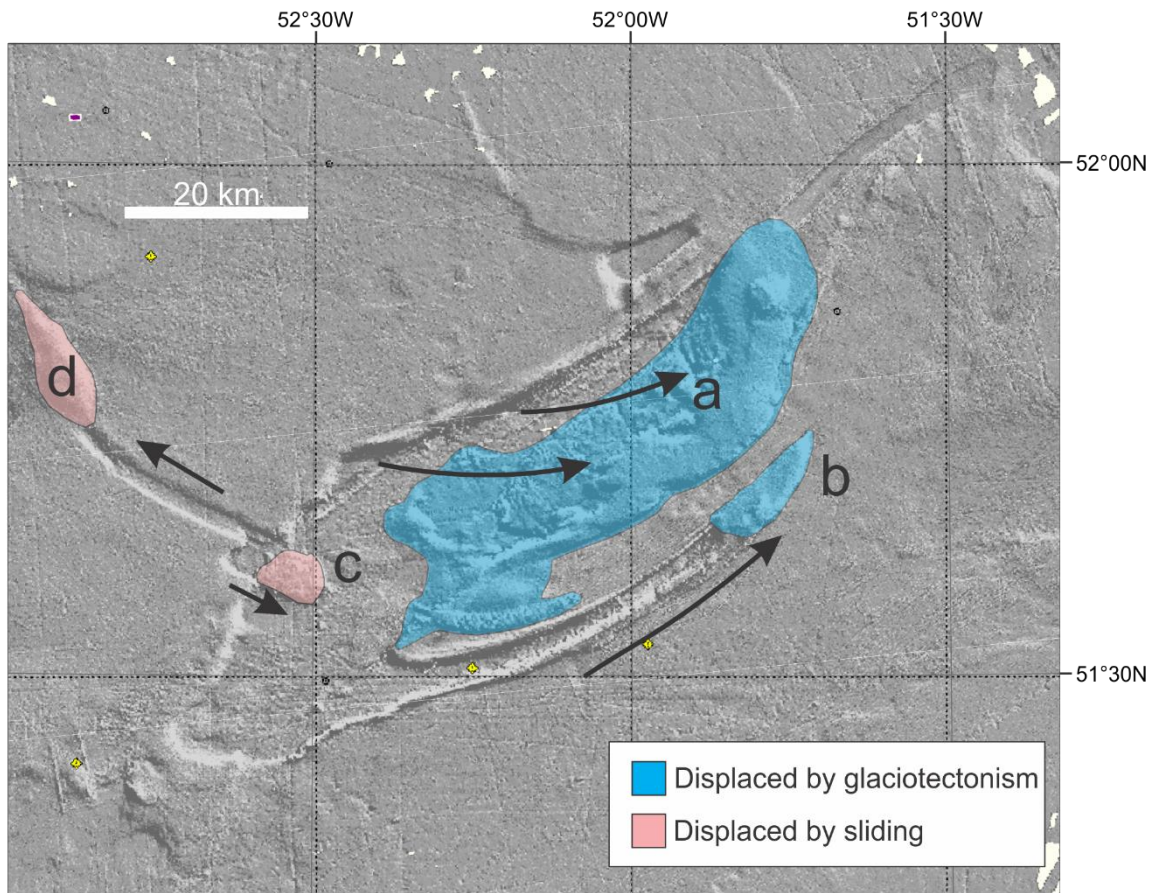


Figure 4. Shaw et al. (2011) interpretation of Olex data, showing geomorphological features in and around NDT. Modified from Shaw et al. (2011) using (November 2017) Olex data.

## 2.4 Glacial history

Continental ice sheets crossed Canada's continental shelf several times over the past 700 ka (Piper, 1988). In the continental shelf stratigraphy, only the Wisconsin glacialiation has been significantly preserved. Large glacialiations would have crossed the entire Shelf, whereas less extensive glacialiations were restricted to channels. The most extensive Wisconsin glacialiation was during isotopic stage 4, and was gradually receding after that. In early marine isotope stage 3, in the Mid Wisconsin, the ice receded to the

present day coastline (Piper, 1988). Then re-advanced to its maximum extent between 30 ka and 21 ka (Tripsanas & Piper, 2008).

## **2.5 Deglacial history**

Shaw et al. (2006) proposed a conceptual model for the deglaciation of the last glacial maximum in Atlantic Canada. Radiocarbon years from Shaw et al. (2006) were corrected using Radiocarbon Calibration – Cal Pal SFCP (2005). During the last glacial maximum ice streams were present in shelf troughs. These ice stream filled troughs include the Laurentian Channel, Bay of Fundy and Notre Dame Channel. Calving, the process by which sea water ablates ice, began at around 23 ka along the Notre Dame Ice Stream. By 21.5 ka and over the next few thousand years, large volumes of ice had succumbed to the ocean, leaving lower elevations of ice on land at the oceans margins. This calving left channels in the ice sheet, allowing for deposition of till tongues by 23 ka. By 17.5 ka the ice sheet was retreating more quickly. Most ice had retreated on land by 16 ka and ablation was dominantly due to melting. Shelf ice caps were no longer present by 13 ka (Shaw et al. 2006).

Shaw and Longva (2017) have a bathymetry-based interpretation of the glacial history as follows. In the Pleistocene grounded ice pushed towards the shelf in a trough, which now underlies the NDT. Stacked sediments from this ice were later subject to glacial erosion, creating the modern NDT. Shaw and Longva proposed that, during the Late Wisconsinan the maximum ice extent was at 30 ka, an ice-flow was present on the Great Northern Peninsula, trending southeast, across the island of Newfoundland. This ice flow had a secondary divide extending off the northeast tip of the island. Catchment areas

from Labrador and Newfoundland sourced the ice for three major shelf-crossing troughs. Catchment areas in southern Labrador, the Great Northern Peninsula of Newfoundland and Notre Dame Bay sourced ice to Notre Dame Trough. Two fast flowing ice-flows converged at the Notre Dame Trough, causing them to undergo ice-stream switching. The northern of these two flows is interpreted to have caused the large area of glaciotectonism (Shaw and Longva, 2017).

## **2.6 Holocene**

Levac et al. (2011) described a palynological record, estimating timing of drainage from the Final Lake Agassiz Flood at 8.3 ka. This record is recorded in Northeast Newfoundland and Scotian shelves at century scale. By comparing their palynological record with four detrital carbonate beds from core HU87033-19 from Notre Dame Channel, Levac et al. (2011) found one of these detrital carbonate beds is coeval with drainage of Lake Agassiz. Changes in dinoflagellate cyst assemblages show the detrital carbonate layers from HU87033-19 indicate meltwater flow over Notre Dame Channel, lowering sea surface salinity by ~10%. (Levac et al., 2011).

Lewis et al. (2012) demonstrated that the detrital carbonate beds, related to the Holocene Final Lake Agassiz Flood, diminish in thickness to the south. They suggested that the Agassiz floodwaters carried icebergs and sediment loads, which the Labrador Current transported south, over the continental margin. Lewis et al. (2012) pointed out two increases in calcite and dolomite in the detrital carbonate bed coeval to the Final Lake Agassiz in core HU87033-19 suggesting that there were two Agassiz floods.

### **3 Materials & methods**

#### **3.1 Shipboard activity**

I was not involved in shipboard activities. The Hudson 2010-023 cruise was to investigate the Notre Dame Trough at the request of Dr. John Shaw. The objectives of the cruise were to improve understanding of Neogene geological history, surficial geology and seafloor properties and processes. The geophysical surveys done on this cruise in the Notre Dame Trough included 360-line km of 1x210 in<sup>3</sup> GI gun seismic and 510-line km of Knudsen sounder (3.5 kHz) chirp. The Hunttec seismic system was inoperable in Notre Dame Trough. Thirteen piston cores were collected.

#### **3.2 Location of cores**

Thirteen piston cores, and all but one with a trigger weight core, were collected from the study area (Fig. 5). Core 1 was taken from the top of the failed block. Core 2 is from a thin acoustically transparent unit over the decollement surface NW of the large failed block. Core 3 is in the higher part of the northwest trending trench NW of the large failed block. Core 4 is from the lower part of the northwest trending trench NW of the large failed block. Core 5 is on the thin edge of the middle mound. Core 6 is in the middle of the south trough. Core 7 is located on the top of the northern ridge of the south trough. Core 8 is on the pinch out of a seismically transparent zone against a decollement surface. Core 9 is on the pinch out of a seismically transparent zone against a decollement surface. Core 10 is on a 20 m high mound in the north trough. Core 11 in an acoustically transparent and stratified section basin on the NE side of Notre Dame Trough. Core 12 is

on a large failure block. Core 13 is on the large block at the west end of the south trough.

Precise locations and water depth of the cores are shown in Table 1.

Table 1. Core localities and water depth.

Core Number	Latitude	Longitude	Water Depth (m)
2010023001	51.596347N	52.526740W	391
2010023002	51.616489N	52.605034W	456
2010023003	51.653668N	52.654722W	414
2010023004	51.632423N	52.578840W	420
2010023005	51.552756N	52.056121W	506
2010023006	51.554992N	52.065583W	526
2010023007	51.361007N	52.090970W	356
2010023008	51.613918N	52.288003W	476
2010023009	51.713797N	52.354072W	476
2010023010	51.753003N	52.148454W	476
2010023011	51.792560N	52.019869W	504
2010023012	51.778324N	52.002016W	466
2010023013	51.660558N	51.828362W	281

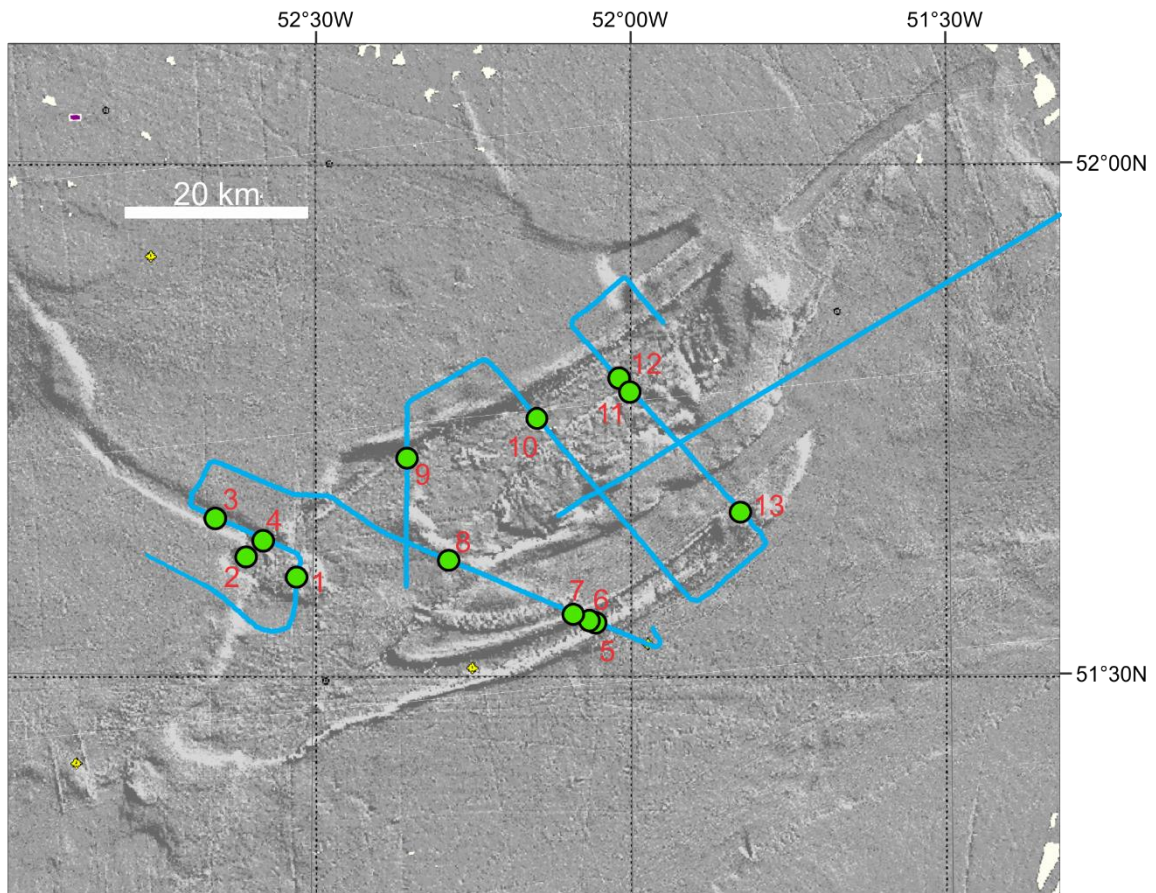


Figure 5. November 2017 Olex data from the outer Notre Dame Trough. Core locations are indicated by green dots, the red numbers beside these dots correspond to the core number. Blue lines show the location of air-gun seismic profiles.

### 3.3 Geomorphology

Interpretation of zones in the NDT was done using November 2017 Olex seafloor images (Fig. 6 on p. 17). These images show a clear image of the seafloor relief in the NDT. The zone interpretations were done with the aid of seismic time profiles from the GI gun data for elevation of structures present in the NDT.

### **3.4 Seismic**

From the 2010023 cruise report, the Knudsen sounder was operated at 12 kHz to gather sub-bottom data when sampling. During transit, or when Hunttec DTS was unavailable, the Knudsen sounder was operated with a 3.5-kHz acoustic signal, allowing for a deep sub-bottom penetration. The 3.5 kHz seismic profiles show good penetration to ~70 ms (50 m) sub-bottom. The GI gun was used to record single channel seismic reflection data. The GI gun seismic profiles show good penetration to 0.4 to 0.45 ms (~300 to 320 m) sub seafloor where a seafloor multiple obscures lower reflectors. Kingdom Suite 8.0.2 was used to interpret both GI gun and 3.5 kHz seismic reflection data under initial supervision of Dr Calvin Campbell.

### **3.5 Core description**

Core descriptions were made using the colour of the core from core photographs received from the Marine Geoscience Collection at the Bedford Institute of Oceanography. Sediment colour was determined visually using the core photos. Core descriptions by Jonathan Roger and X-radiographs were used in determining presence of IRD. X-ray fluorescence (XRF) was used on cores 2, 3, 8, 11 and 12 to determine elemental abundance for correlation. Spectrophotometry was used to measure colour reflectance, expressed by  $L^*$ ,  $a^*$ , and  $b^*$  values. Variation in  $a^*$  was used in differentiating subtle differences in sediment colour.

### **3.6 Portable X-Ray fluorescence (pXRF)**

XRF is a method of whole rock chemical analysis which emits short-wavelength X-rays onto the sample. These short-wave X-rays ionize the atoms in the sample, causing

an inner electron to leave its shell and an outer electron to drop into its place. This movement of an outer electron to an inner shell causes the atom to release a secondary X-ray photons through a phenomenon called fluorescence. The wavelength this secondary X-ray photon corresponds to the element which released it. The Innov-X system Delta Premium XRF spectrometer was used for XRF analysis. The cores were prepared with Glad Wrap™ and analyzed with soil mode. The elements analyzed are Ti, V, Cr, Mn, Fe, Ni, Cu, Zn, As, Se, Rb, Sr, Y, Zr, Nb, Mo, Ag, Cd, Sn, Sb, W, Hg, Pb, Bi, Th, U, Co, P, S, Cl, K, and Ca in parts per million (ppm). The elements examined in more detail are Ca, K, Rb, Zr and Ti. This data was recorded in Excel, where the Ca/Ti, K/Ti and Zr/Ti ratios were calculated to normalize the data to reduce the effects of variable density and water content. Ca/Ti is used to indicate carbonate minerals; K/Ti is used to indicate clays present, as they contain K in their structure; Zr/Ti can be used to indicate sand, as zircon grains are often present in quartz sand. Rb (ppm) vs K<sub>2</sub>O (wt%) was plotted in attempt to determine if the source was rich in micas or feldspars. Sr vs Ca was plotted to help determine provenance as plagioclase should contain a higher Sr/Ca ratio than calcite.

### **3.7 Spectrophotometry**

Spectrophotometry is a non-destructive analysis method done to determine the colour variation of sediment downcore. The spectral data use the CIE (La Commission Internationale de l'Eclairage) L\*, a\*, b\* colour system. L\* is how bright the colours are, with low values being closer to black and high values being closer to white. The a\* and b\* show the colour of the system. The a\* goes from green at low values to red at high values; b\* goes from yellow at low values to blue at high values (Debret et al., 2011). This study examined L\* and a\* downcore.

### **3.8 Raw data**

Data are archived in the Marine Geoscience Collection of the Geological Survey of Canada ([http://ed.gdr.nrcan.gc.ca/index\\_e.php](http://ed.gdr.nrcan.gc.ca/index_e.php)). This data is partly available through the expedition database and partly by request to the curator.

## **4 Results**

### **4.1 Morphology**

Geomorphologically the Notre Dame Trough study area has seven zones (Fig. 6). From north to south these are: North Ridge, North Trough, Middle Mound, Undisturbed, Middle Ridge, South Trough and South Ridge. The north and south sides of the trough are bounded by relatively undisturbed sea floor. The North Ridge is the topographic high which extends along the north side of the North Trough. This North Ridge lacks a berm near the slump block on the west side of the study area. The North Trough is a topographic low in which there are two discontinuous berms. At the southern edge of the North Trough is the topographically higher and rough Middle Mound. The Middle Mound is a sediment pile in the centre of the study area. Towards the south-west the Middle Mound begins to taper into a berm. Near the south-west edge of the Middle Mound, it transitions into the Middle Ridge. The Middle Mound and Middle Ridge enclose the Undisturbed zone within the trough. The Undisturbed zone is a topographically flat area with no berms and is at a higher elevation than the troughs. The Middle Ridge is a berm which extends along the top of the north side of the South Trough. The South Trough is a topographic low between the Middle and South ridges.

The South Ridge is a berm along the south side of the South Trough. The South Ridge becomes broader toward the north-east, where it extends further than the South Trough.

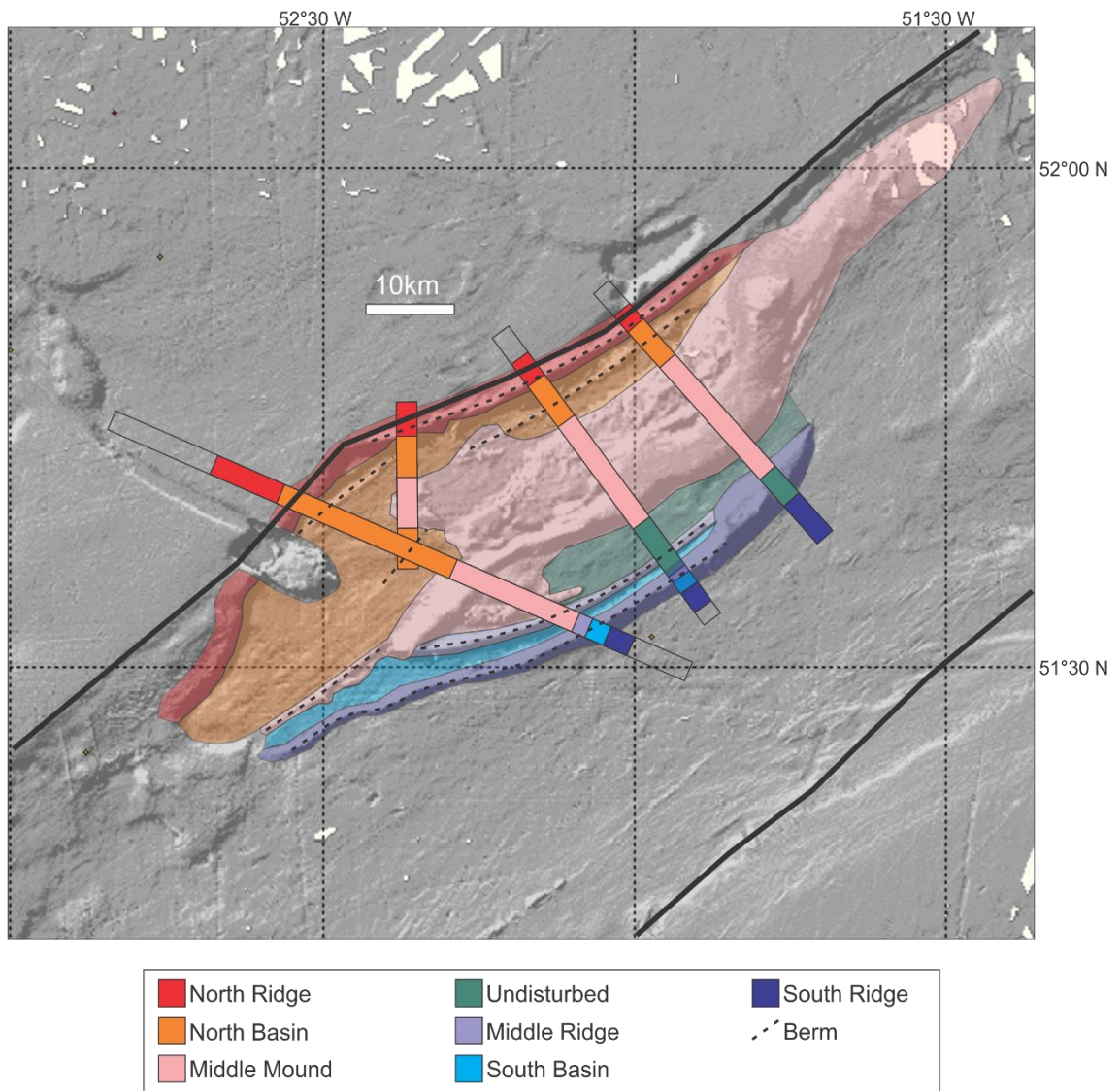


Figure 6. November 2017 Olex data from the Notre Dame Trough, showing division into morphological regions. The coloured lines across the image are seismic lines which were used for elevation of the zones to determine where the boundaries between zones are. The lateral extent of Notre Dame Trough is depicted by thick black lines.

## 4.2 Seismic Reflectors

### 4.2.1 GI gun

The GI gun seismic profiles reveal a major reflector that can be traced throughout most of the region, traced as the green horizon (Fig. 7 s-t). This major reflector is a regional unconformity, which for this paper will be called the Notre Dame Unconformity. Four dipping surfaces which truncate weak reflectors can be traced below the major unconformity, and dip toward the continental slope (Fig. 7 s-t). Attempts to trace these horizons down the continental slope were unsuccessful. The ridges bordering basins within NDT show a layer of incoherent seismic data, interpreted to be till, between relatively flat-lying reflectors. Within this till are some faint reflectors which dip toward the basin of the trough; this till then leads into wedging structures which lead into mounds of till (Fig. 7 d-e). On the north-east side of NDT behind the North Ridge is a depression which truncates the drawn blue horizon and overlying reflectors (Fig. 8 o-p). Highlighted orange in Figure 8 (o-p) is incoherent seismic, interpreted to be till, sitting directly above the Notre Dame Unconformity. The Middle Mound shows a staircase structure on the SE side, where seismic reflectors are cut off by incoherent seismic, however below the incoherent seismic and the truncated flat-lying reflectors are

continuous reflectors (Fig. 8 k-l).

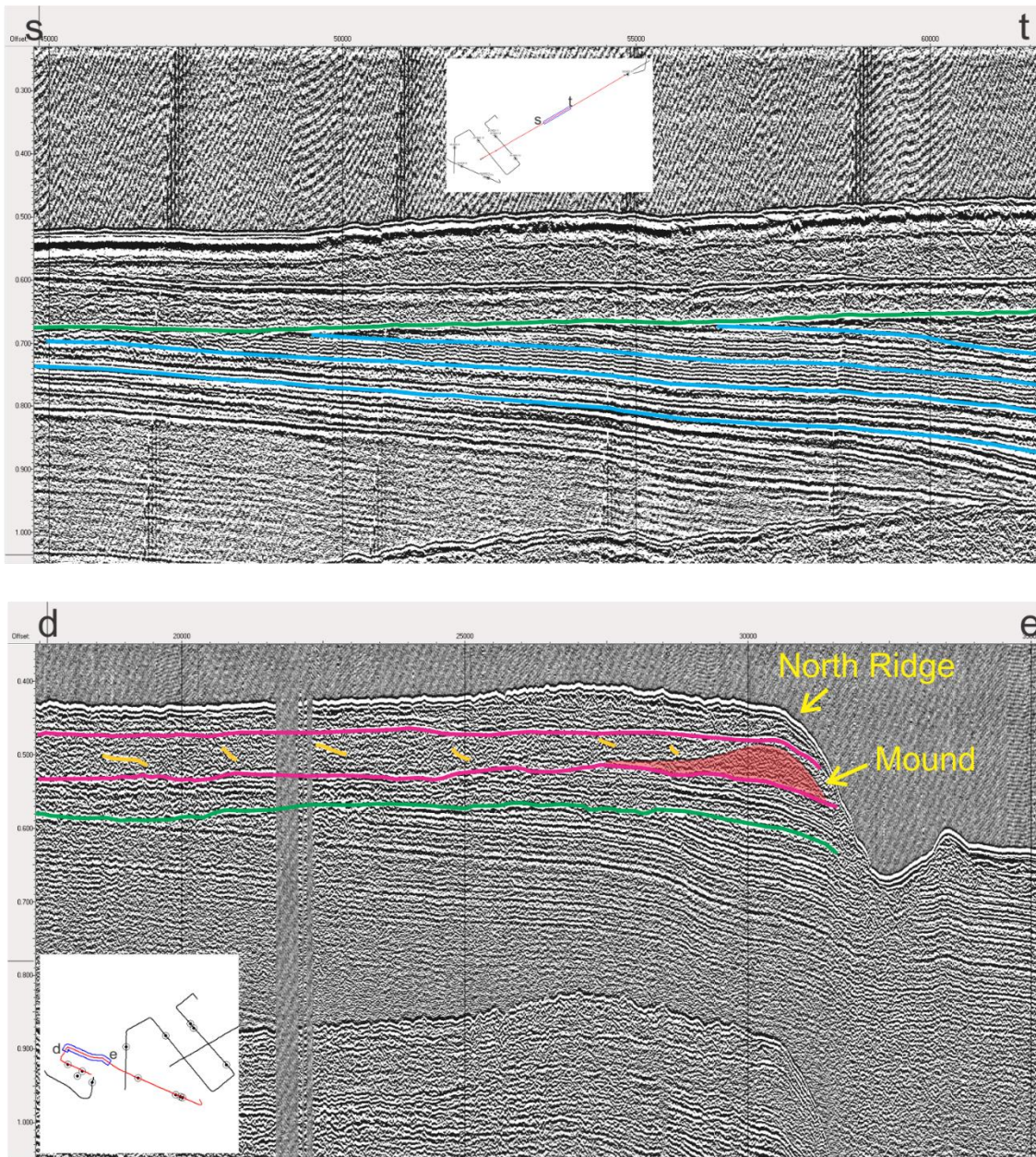


Figure 7. s-t) The green horizon is the Notre Dame Unconformity. The Notre Dame Unconformity truncates the top of shallow dipping reflectors, which are highlighted in blue. d-e) Sediment mound, in red, at the end of relatively incoherent seismic with some dipping reflectors, highlighted yellow, in the incoherent seismic. These yellow are interpreted to be small till deltas.

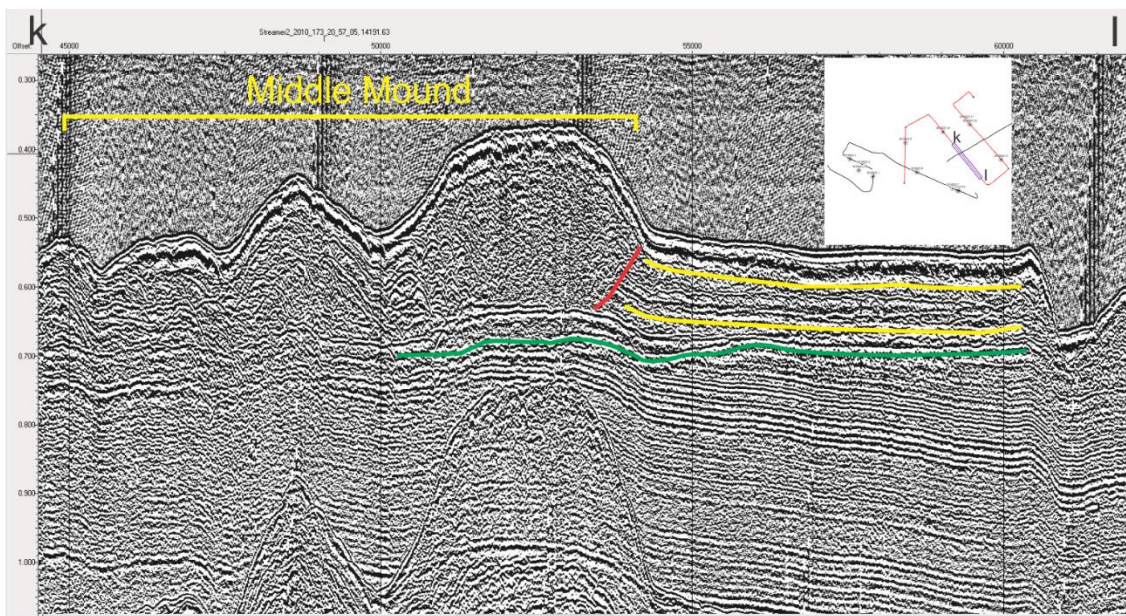
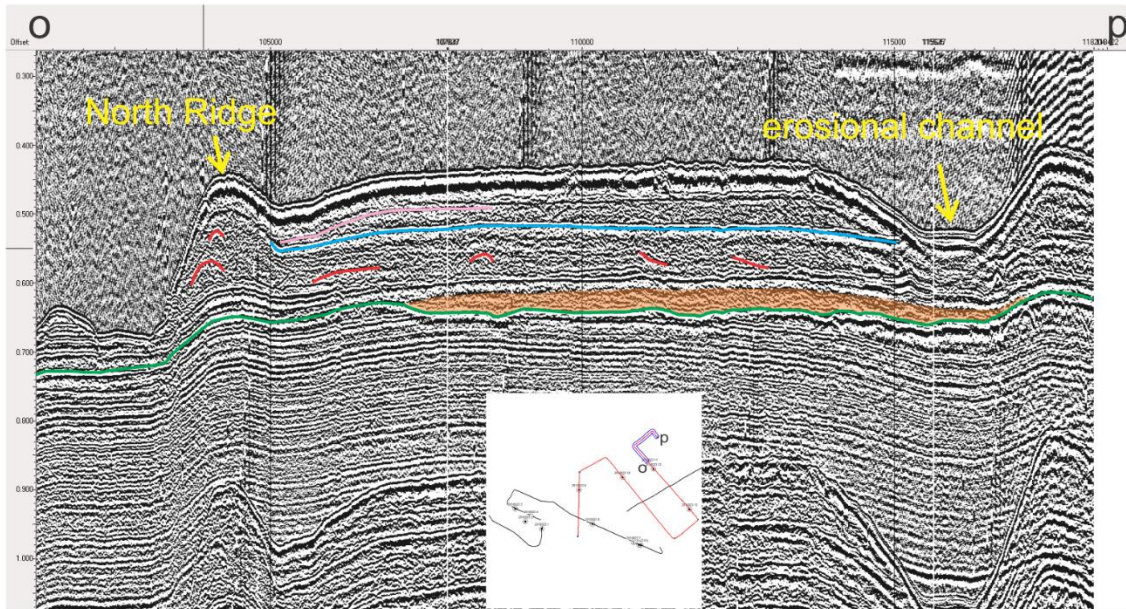


Figure 8. o-p) A erosional channel near the North Ridge. This erosional channel truncates the blue reflector. Faint reflectors in the incoherent seismic are marked with red. k-l) Flat-lying reflectors (yellow) truncated (red) by incoherent seismic reflections within the Middle Mound.

Towards the shelf edge the dipping reflectors which are truncated by the Notre Dame Unconformity also begin to truncate against each other (Fig. 9 u-v). At the shelf edge these dipping beds show downlap against a shallow dipping reflector. This shallow dipping reflector is interpreted to be a previous shelf edge and is cut off by a multiple.

Also at the shelf edge, reflectors, such as the Notre Dame Unconformity, show clinoforms. The downlap and presence of clinoforms and incoherent seismic facies suggests these dipping reflectors near the shelf are till deltas (Fig. 9 v-w).

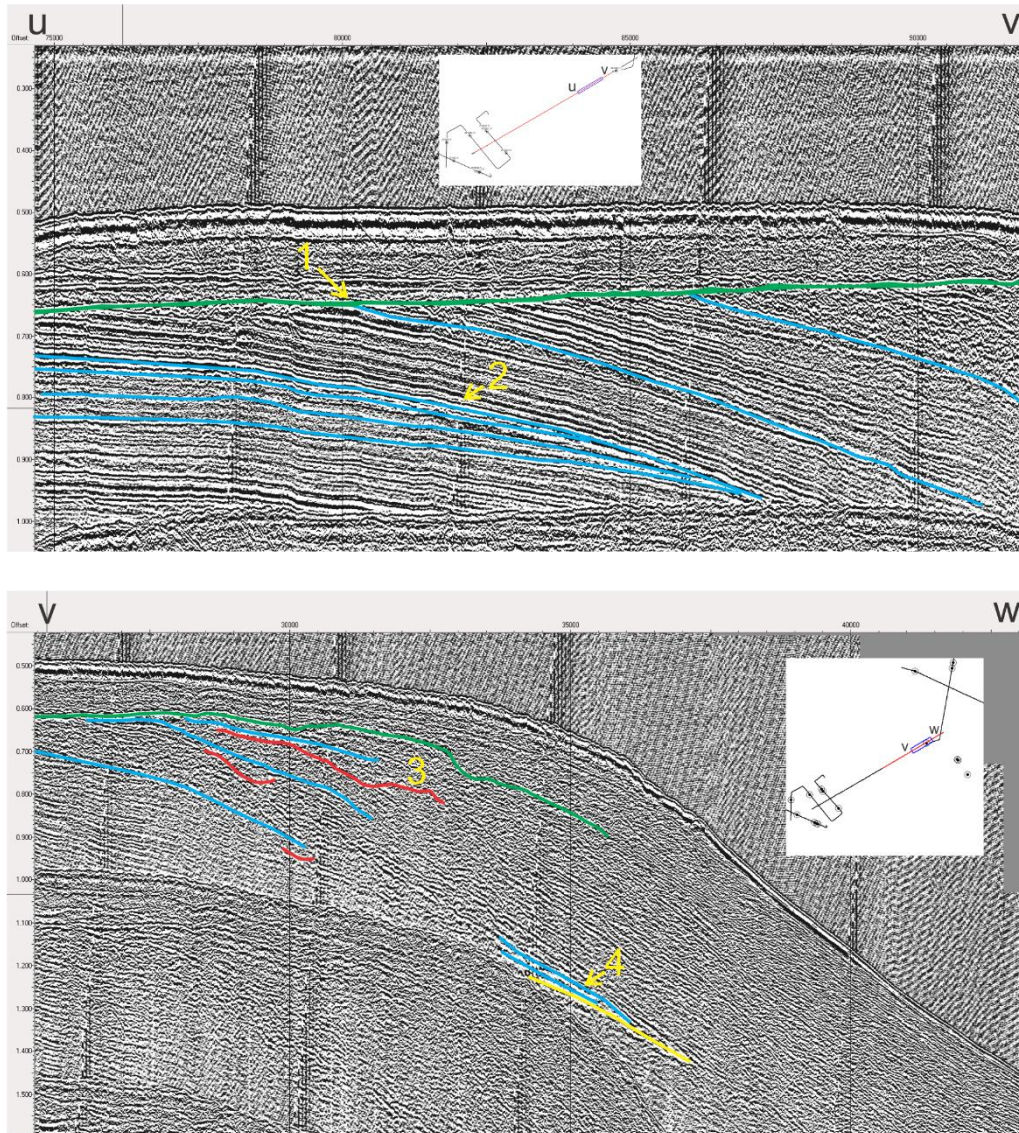


Figure 9. u-v) Truncation of dipping reflectors (blue) by Notre Dame Unconformity (green) (1). Dipping reflectors truncated by other dipping reflectors (2). In the v-w section the green line is a continuation of the Notre Dame Unconformity, the blue lines are continuations of dipping reflectors and the red lines are irregular reflectors showing clinoforms (red) (3). Blue reflectors shown to be downlapping on yellow reflector, interpreted to be a previous shelf edge (4).

At the base of the NE Newfoundland Slope seaward of the Notre Dame Trough there are mass transport deposits (MTD) described by Campbell (2005). Seismic reflectors in mass transport deposits at the edge of this fan are similar to those of the MTDs of Campbell (2005) in Orphan Basin (Figure 9). Attempts to correlate the reflectors seaward of NDT with the dated reflectors from Campbell (2005) were unsuccessful. Tracing the major unconformity horizon downslope shows a similar seismic time to the MTD horizons at the edge of the fan. The horizons which were drawn in an attempt to connect with Campbell (2005) were either obscured or cut off by erosion at Orphan Spur. Jump correlations between a reflector in the glacial fan (blue in Fig. 10) and Campbell (2005) suggest that the reflector may either be the equivalent to the Blue (30-40 ka) or Red (235 ka) reflector in Orphan Basin from Campbell (2005).

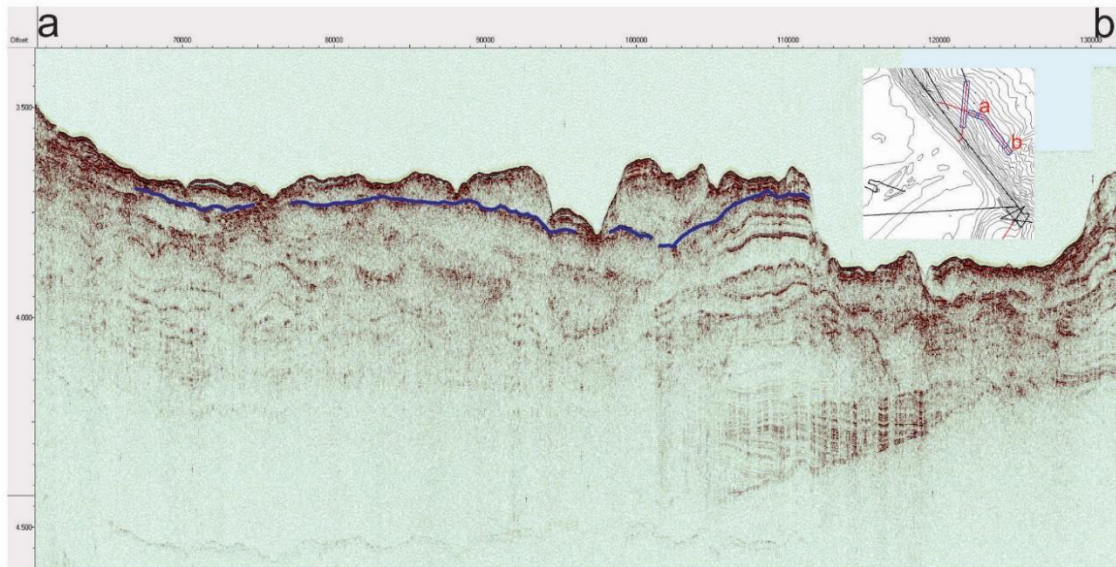


Figure 10. The base of the continental slope off the Northeast Newfoundland shelf seaward of Notre Dame Trough showing the blue horizon.

### **4.2.2 Seismic Facies**

There are three main seismic facies in the study area. Facies 1 is as a laterally continuous incoherent facies with some faint dipping reflectors (Fig. 11 j-k). This facies shows wedging below the ridges. Facies 2 is an incoherent facies which lacks any strong reflections (Fig. 11 k-l). Facies 3 is continuous dipping subparallel reflections which largely dip toward the shelf edge (Fig. 11 s-t).

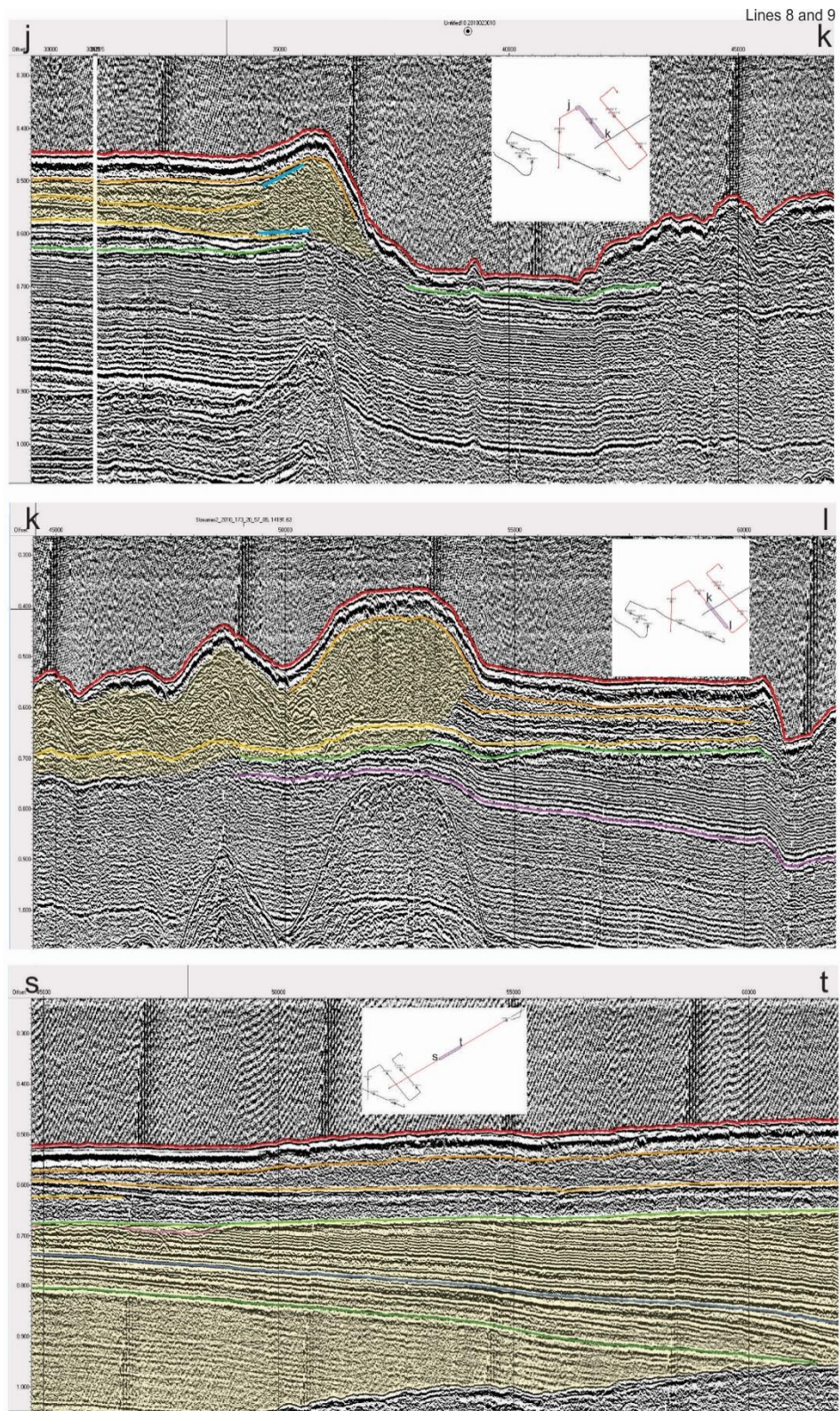


Figure 11. the highlighted section shows the facies. Section j-k is facies 1. Section k-l is facies 2. Section s-t is facies 3.

### 4.2.3 Seismic units

There are five seismic units in the study area. Unit 1 (Fig. 12) is comprised of seismic facies 1 and its confining flat-lying reflectors. This unit is present above the Notre Dame Unconformity under the flat topography of the sea floor near the ridges and in the undisturbed zone in figure 6. Unit 2 occurs above the Notre Dame Unconformity and includes the wedging portion of seismic facies 1 and the dipping reflectors lateral to the ridges. Unit 3 (Fig. 12) consists of facies 2 and occurs above the Notre Dame Unconformity in the Middle Mound. Unit 4 (Fig. 12) consists of facies 3 and is present below the Notre Dame Unconformity. Unit 5 exists laterally to Unit 4 and is comprised of facies 3, however the dipping beds of Unit 5 which are dipping down the continental slope are less coherent than those in Unit 4.

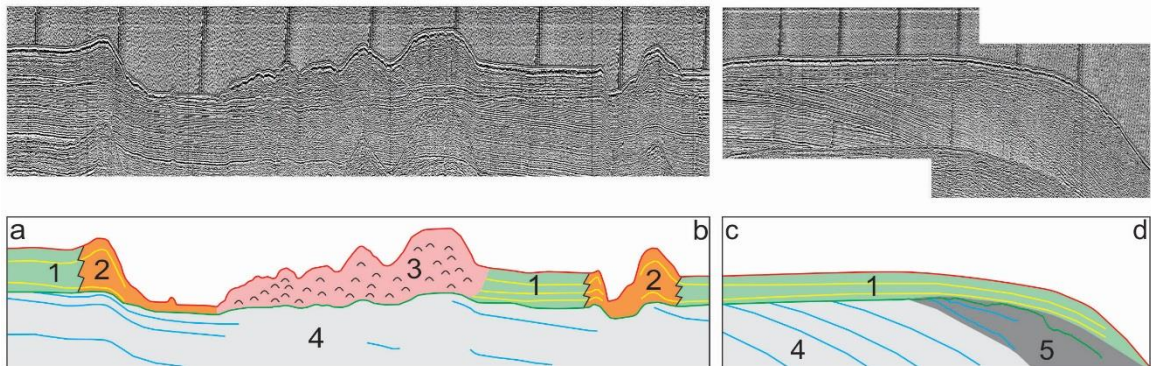


Figure 12. seismic units. The section a-b is taken perpendicular to NDT. The c-d section is taken on the shelf break.

### 4.2.4 Knudsen 3.5 kHz profiles

The 3.5 kHz seismic profiles from the basins show up to two strong subparallel discontinuous sub-bottom reflections (Fig. 13). These reflectors are interpreted to be major changes in the muds. Cores 5, 6, 8, 9, 11 and 12 are taken from the top of these two mud reflectors. Seismic profiles occasionally show concave downward reflections which

are interpreted to be due to dropstones; these reflections are especially prevalent in the mound which core 13 was taken from. Cores 1, 7 and 13 penetrate these reflectors (Fig. 12). The 3.5 kHz for cores 2, 3, 4 and 10 does not show any reflectors.

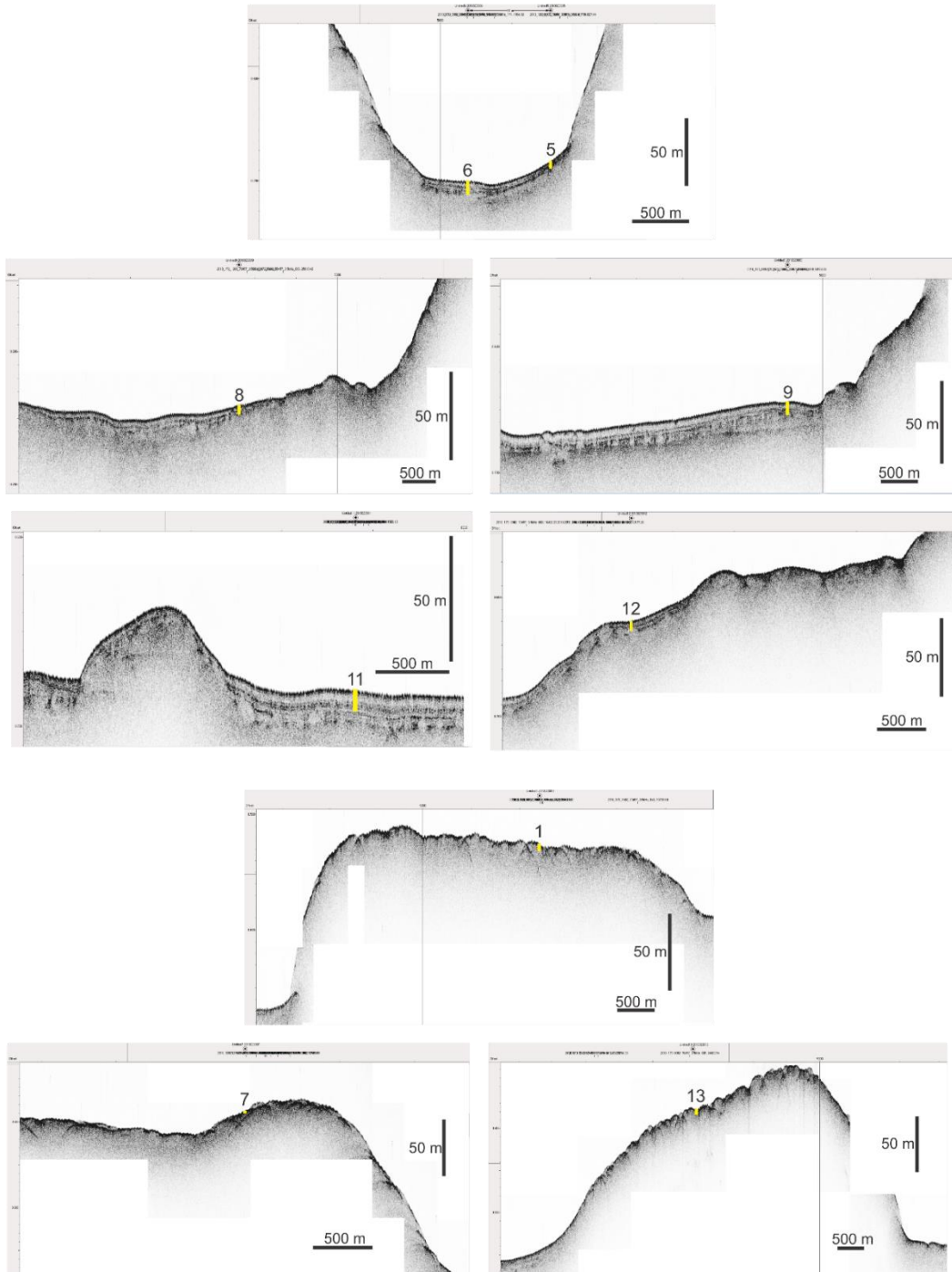


Figure 13. 3.5 kHz profiles showing core locations (numbers). Core lengths shown to scale.

## **4.3 Lithostratigraphy**

### **4.3.1 Introduction**

To understand the cores, the lithostratigraphy was broken up into Units A, B, C, D, E, F, and G. Unit A is an olive grey mud, which is the surface unit in all cores. Unit B is defined by its high Ca/Ti ratio and is also mainly an olive grey unit with occasional tan beds. The top of the highest tan coloured interval marks the boundary between units A and B. Unit C is defined as primarily brown muds containing little to no IRD below the lowest tan mud. The base of unit C is where the brown, red or grey mud with no IRD passes into muds with significant IRD. Unit D defined by mottled red, grey and dark-brown to black muds containing abundant IRD. Unit D in cores 1, 5, 6, 9, 11 and 12 has a distinct bright red mud bed. The top of Unit D is typically a red mud that contains more IRD than the overlying grey or brown muds of Unit C. Unit E is compact red muds with shear strength values of ~30 kPa. Unit F is highly compact muds with shear strengths exceeding 100 kPa. Unit G, present only in core 2, shows a gradual increase in shear strength from 10 kPa to ~35 kPa.

### **4.3.2 Core descriptions**

Core 11 (Fig. 14e on p.43) was used as a reference core to define sediment units A-D that could then be correlated between the piston cores. Core 11 is from a basin on the NE side of Notre Dame trough, in a water depth of 504 m. Unit A consists of olive grey mud with bioturbations, a sand bed at 40 cm and occasional ice-rafted detritus (IRD) to 115 cm. Unit B (115 to 508 cm) consists of a tan mud with bioturbations, a high Ca/Ti ratio and some IRD to 274 cm. This tan mud contains more abundant IRD from 165 to

185 cm and from 265 to 274 cm. An olive grey mud to 326 cm; tan mud with a high Ca/Ti ratio and IRD to 333 cm; olive grey mud with to 414 cm which has peaks in Zr/Ti and Rb/Ti at 355 cm and a sandy bed at 395 to 400 cm; brown mud with abundant IRD to 487 cm which has a sandy bed at 422 cm and a bioturbated base; tan mud with a high Ca/Ti ratio and abundant IRD to 508 cm. Unit C (508 to 790 cm) consists of a weakly layered bioturbated brown mud lacking IRD to 699 cm; grey mud containing some shells to 770 cm. The base of Unit C grades into red muds of Unit D, with an increase in IRD. Unit D (770 to 878 cm) consists of red mud with abundant IRD to 852 cm; A distinctive bright red mud bed with abundant IRD to 853 cm; laminated red muds with red and grey speckles of mud to 878 cm. Two black beds are present at 870 to 872 cm and 873 to 878 cm. Unit E, defined in core 12, is not present in this core.

Core 12 (Fig. 14e) is most like core 11 of the cores studied, and is located ~2 km NW of 11 in the same basin. Unit A (0 to 25 cm) consists of an olive grey mud. Unit B (25 cm to 166 cm) consists of a tan mud containing IRD to 128 cm; an olive grey mud to 143 cm; brown mud with IRD to 158 cm; a tan mud with IRD to 166 cm. Unit C (166 to 310 cm) consists of a brown mud, which contains a few pebbles to 250 cm; grey mud to 310 cm. Unit C in core 12 is thinner than in core 11, but is otherwise similar. Unit D (310 to 448 cm) consists of red mud layered with wispy black mud beds and abundant IRD to 447 cm. The black beds are not present at the top of Unit D in core 11, but similar black muds are present at the bottom of core 11; Unit D in core 12 is otherwise like that of core 11. From 310 cm to 445 cm there are red and black speckles of mud. Unit D has a distinct bright red mud bed at 396-400 cm. Unit E in core 12 is defined from 448 to 550 cm, and is red muds that are more compact with higher shear strength of about ~30 to ~60 kPa, compared to ~10 kPa higher in the core. Unit F is also defined in core 12, from 550 cm to

the base of the core at 589 cm, with compact red muds showing an abrupt increase in shear strength to ~200 kPa. Units E and F in core 12 show high values of Ti ppm and Rb ppm which is not present in the high shear Unit G strength zone of core 2.

Core 9 (Fig. 14d) is the next most like core 11 and is located ~25.9 km WSW from core 11 the same basin on the northern side of NDT. Unit A (0 to 53 cm) consists of an olive grey mud. Unit B (53 cm to 232 cm) consists of a tan mud which contains a few pebbles of IRD and extends to 90 cm; an olive grey mud which extends to 152 cm; brown mud to 222 cm; grading into a tan mud bed which extends to 232 cm. Unit B in core 9 is like that in core 12. Unit C (232 to 450 cm) consists of a brown mud with little IRD to 359 cm; a red mud that little IRD to 455 cm. Unit C differs from Unit C in cores 11 and 12 in that it has red mud instead of grey mud at the base. Unit D (455 to 615 cm) consists of brown muds with abundant IRD and contains rare grey mud clasts to 615 cm. Below 615 cm is Unit E as the shear strength of the core rapidly increases from ~20 kPa to ~35 kPa. Unit E consists of the same lithology as Unit D to the end of the core at 778 cm. At 639 cm, there is a distinct bright red mud bed, which is interpreted to be the same distinct red mud as seen at 852 cm to 853 cm in of core 11.

Core 6 (Fig. 14c) is located in a basin on the SW side of NDT ~25.8 km SSW of core 11. Unit A (0 to 56 cm) consists of an olive grey mud. Unit B (56 to 124 cm) consists of a tan mud with some IRD to 90 cm; olive grey mud with some IRD to 124 cm; brown mud to 205 cm; a tan mud to 223 cm. This tan mud is assumed to be the equivalent to the tan interval in core 11 at 490 cm to 508 cm, although it contains significantly less IRD. Unit B is much thinner than Unit B in cores 9 and 12 and one of the tan beds seen in core 11. Unit C (223 to 307 cm) consists of a brown mud which extends to the base of Unit C at 307 cm. Unit D (307 to 727 cm) consists of a red mud containing IRD to 356

cm; red mud becomes layered with beds of dark-brown mud and less IRD to 412 cm; brown mud containing abundant IRD and large grey mud clasts to 605 cm. At 597 cm this brown mud has a distinct bright red mud bed, which is interpreted to be the same red mud bed as that seen in core 11 from 852 cm to 853 cm. From 605 to 643 cm is a layered brown mud containing little IRD; grey mud with IRD to 664 cm; bedded red and brown muds with some IRD and small red mud clasts to 727 cm. Unit E (727 to 966 cm) consists of a massive red mud containing brown and red mud clasts to 767 cm; a brown mud with large grey and red mud clasts to the base of the core at 996 cm. The lower red mud unit becomes browner with depth, contains fewer mud clasts with depth and has a higher shear strength than the above muds. Shear strength in Unit E increases from ~15 kPa near the top to ~30 kPa at the base; for comparison the overlying Unit D has shear strength values more typically ~10 kPa.

Core 5 (Fig. 14c) is located upslope from core 6, and ~25.9 km SSW of core 11. Unit A is 24 cm thick, this is shorter than Unit A in cores 6 and 11. The top of core 5 is 24 cm of an olive grey mud. Unit B (24 to 115 cm) consists of a tan mud to 63 cm and contains some granules; olive grey mud to 73 cm; grey mud not present in cores 6 or 11 to 89 cm; a massive brown mud containing some IRD to 107 cm; a tan mud to 115 cm. This tan mud is assumed to correlate with the tan layer in core 11 at 490 cm to 508 cm, however this tan layer in core 5 lacks IRD unlike the core 11 counterpart. Unit C (115 to 235 cm) consists of a brown mud with little IRD to 235 cm. Unit D (235 to 545 cm) consists of a red mud to 255 cm; red mud bedded with brown mud to 271 cm; a massive brown mud with large grey mudclasts to 510 cm, this brown mud has a bright red mud bed 447 cm; brown mud with large red and grey mud clasts until the end of core at 545 cm.

Core 2 (Fig. 14b) is located nearby cores 1, 3 and 4, and ~46.2 km WSW of core 11. Unit A (0 to 10 cm) consists of an olive grey mud. Unit B (10 to 217 cm) consists of a tan mud which contains pebbles to 55 cm; an olive grey mud with sand beds to 136 cm; tan mud containing IRD to 144 cm. This thin tan layer is assumed to be the same tan layer in the olive grey muds as the one in core 11 from 326 cm to 333 cm. From 144 to 200 cm is an olive grey mud with many sandy beds and an overall low Ti ppm. These sandy beds in the lower olive grey muds of Unit B are more prominent than those in core 11. From 200 to 210 cm a brown mud; a tan mud with IRD to 217 cm. Unit C (217 to 221 cm) consists of a brown mud to 221 cm. Unit D (221 to 325 cm) consists of a red mud which contains abundant pebbles and brown mudclasts to 281 cm; a red mud bedded with brown mud to 325 cm. Unit G (325 to 671 cm) consists of compact brown mud containing few pebbles to 359 cm; compact brown mud with abundant IRD to 413 cm; compact red mud that contains abundant pebbles to 671 cm. Unit G of core 2, unlike Units E and F of core 12, shows a more gradual increase of shear strength downcore. Also differentiating Unit G from Units E and F is the lower Ti ppm and Rb ppm values in Unit G. Unit G differs from Unit D in core 2 by having a lower Rb ppm and a higher K<sub>2</sub>O wt % (Fig.v).

Core 8 (Fig. 14d) is in a basin in the northern trough, ~27.4 km SW of core 11. Unit A (0 to 45 cm) consists of an olive grey mud. Unit B (45 to 126 cm) consists of a tan mud containing IRD to 78 cm; olive grey mud to 105 cm; brown mud to 110 cm; a tan mud containing IRD to 126. Unit C (126 to 212 cm) consist brown mud with occasional grey beds and very few granules to 212 cm. Unit D (221 to 375 cm) red mud with abundant IRD to 250 grey mud to 282 cm; maroon mud to 297 cm; grey mud to 375 cm; grey mud bedded with red and maroon muds to 409 cm; grey muds to 511.5cm. Unit D in

core 8 has different colours of mud than core 11, however the abundant IRD and therefore classifies as Unit D.

The grey mud present in Unit D of cores 6 is likely a mud clast and differs from the grey muds of core 8. In core 6, shear strength spikes to 123 kPa in the grey mud from 643-664 cm, shear strength immediately drops after this spike. If this shear strength were due to grounded ice, then this decrease in shear strength down core should be more gradual. Core 5 is in close proximity to core 6 and contains compact grey muds which are clearly mud clasts in Unit D. Two peaks in shear strength in core 5 of 70 kPa and 60 kPa are present at 316 cm and 342 cm respectively, at both of these depths are compact grey mud clasts. This further suggests the grey mud seen in core 6 is a large grey mud clast. The grey muds of core 8 do not show an increased shear strength. The grey muds in core 8 may be due to reduction or are older muds as core 8 is taken over a decollement surface.

Core 10 (Fig. 14e) is located in the northern trough ~10.8 km WSW of cores 11 and 12. Unit A (0 to 12 cm) consists of olive grey mud. Unit B (12 to 26 cm) consists of tan mud with IRD to 26 cm. Unit D (26 to 75 cm) consists of brown mud containing IRD which is coarser down core. Large clasts of red mud from 67 cm to 84 cm. Unit E (75 to 146 cm) consists of brown mud with IRD to 118 cm; a light tan mud containing IRD to 120 cm; brown mud with IRD to 146 cm. Below 75 cm this core shows a rapid increase in shear strength from ~3 to ~30 kPa.

Core 7 (Fig. 14c) is on the Middle Ridge, upslope from cores 5 and 6, and ~25.5 km SSW from core 11. This core has abundant IRD throughout every unit. Unit A (0 to 10 cm) consists of a sandy olive grey. Unit B (10 to 49 cm) consists of a light grey mud to 16 cm; a pinkish tan mud to 25 cm; a light grey mud to 49 cm. The pinkish-tan mud and grey mud in Unit B are not matched in core 11. Unit C (49 to 74.5 cm) consists of a dark-

brown mud to 74.5 cm. Unit D (74.5 to 193 cm) consists of red muds to 185 cm; brown muds to 191 cm; brown sands to 193 cm. Both piston core and trigger weight core for core 7 are short. The cutter at the bottom of the piston core 7 is not broken. Because the bottom of core 7 is sand, it likely did not hit a rock and the momentum of the piston core was stopped by this sand.

Core 1 (Fig. 14b) is located on top of the slide block at the west side of the NDT ~42.4 km WSW of core 11. Unit A (0 to 16 cm) consists of a silty olive grey mud which contains some granules. This core does not have a Unit B or Unit C. Unit D (16 to 345 cm) consists of a brown mud with IRD and the rare red mud clast to 345 cm. There is a disturbed bright red mud bed at 108 cm to 110 cm. This bright red mud bed is used as justification for calling these brown muds Unit D, as a distinct red mud layer appears in core 11 in Unit D. At 345 cm the brown mud appears very compact and shear strength values increase from ~20 kPa to ~200 kPa. These high shear strength muds mark Unit F which extends from 345 cm to the end of the core at 404 cm. Unit E is not present in this core however.

Core 3 (Fig. 14b) is located in the trench trending NW from NDT, ~48.2 km WSW of core 11. Unit A (0 cm to 10 cm) consists of an olive grey mud. Unit B (10 to 21 cm) consist of a tan mud with IRD. Unlike the Unit B of core 11, Unit B of core 3 consists of a tan mud. This tan mud contains wisps of olive grey mud and contains a few granules. There is no Unit C in this core. Unit D (21 to 328 cm) consists of a red mud with abundant IRD.

Core 4 (Fig. 14b) is located in the northern trough ~44 km WSW of core 11. Unit A (0 to 14 cm). consists of an olive grey mud to 14 cm, with a few pebbles near the bottom. Units B and C are not present in this core. Units B and C are not present in this

core. Unit D (14 to 170 cm) consists of a red mud containing pebbles to 85 cm; red mud with brown mud beds to 170 cm. Based on the pebbles in the uppermost red muds of Unit D followed by the bedded red muds, this could be the top of Unit D as seen in core 11. Unit E (170 to 343 cm) consists of a compact brown mud with a large amount of IRD and some red and grey mud clasts. This is defined as Unit E as the shear strength increased from ~20 kPa to ~35 kPa below 170 cm.

Core 13 (Fig. 14c) is located at the east end of the south trough, ~18.2 km SE of core 11. Unit A (0 to 45 cm) consists of a sandy olive grey mud to 45 cm. This olive grey unit gets lighter coloured with depth until it ends at 45 cm. Units B and C are not present in this core. Unit D (45 to 159 cm) consists of red muds with abundant IRD to 159 cm. Unit E (159 to 267 cm) consists of red muds with abundant IRD. This is defined as Unit E as the shear strength increases from ~10 kPa to ~35 kPa below 159 cm.

Colour Legend

	Olive grey mud
	Olive grey sandy mud
	Olive grey mud with IRD
	Layered red mud
	Red mud with IRD
	Brown mud
	Layered brown mud
	Brown mud with IRD
	Grey mud
	Grey mud with IRD
	Tan mud
	Sand
	Gravel

Symbol Legend

Dateable shell	
Bioturbation	
Mud clast	
Lamination/thin beds	

Figure 14a. Core plot legend. Symbols provided by GSC.

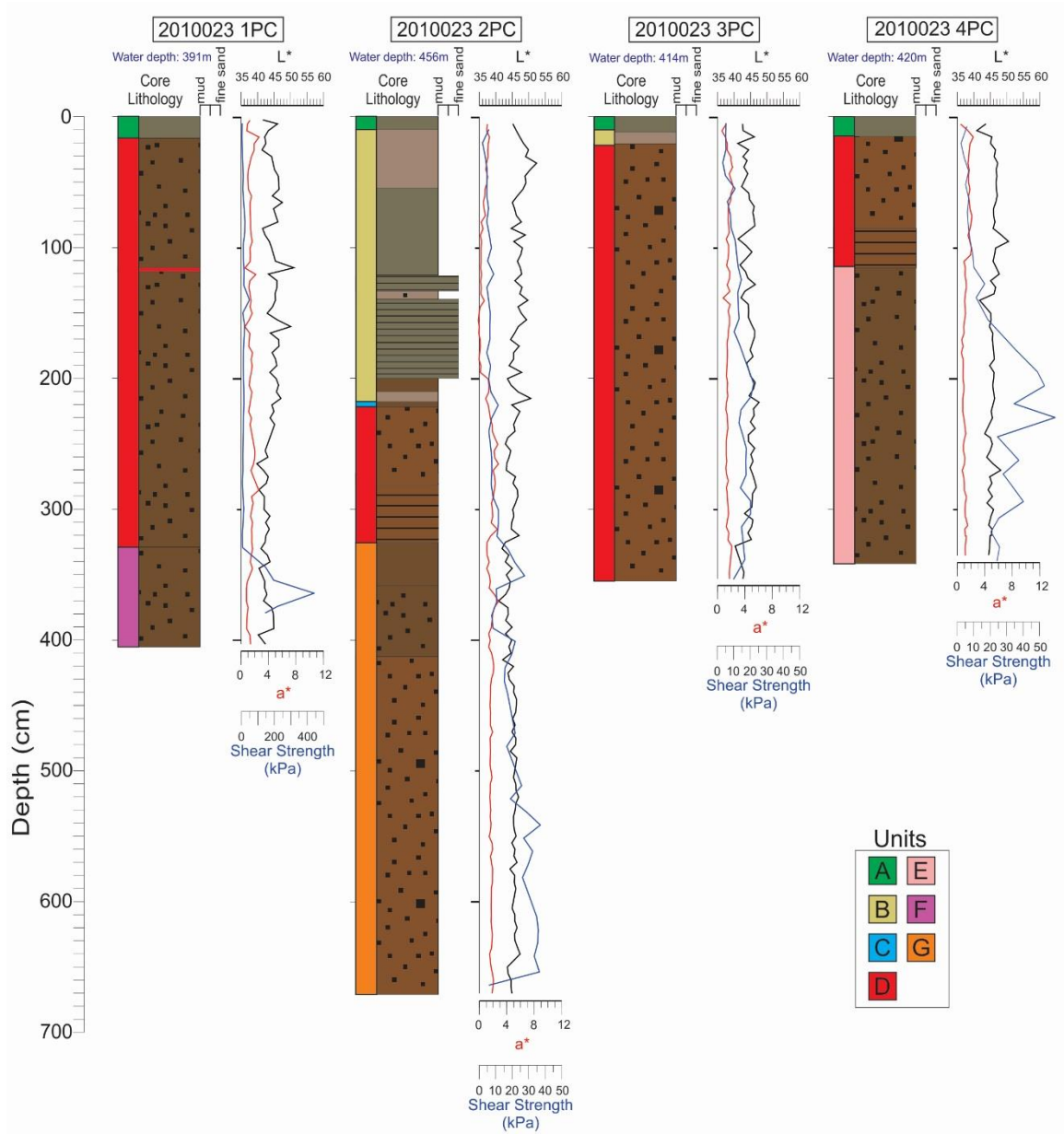


Figure 14b. Downcore summary plot for cores 1, 2, 3 and 4. Cores are plotted together based on their geographic proximity. Note change of scale for shear strength in core 1.

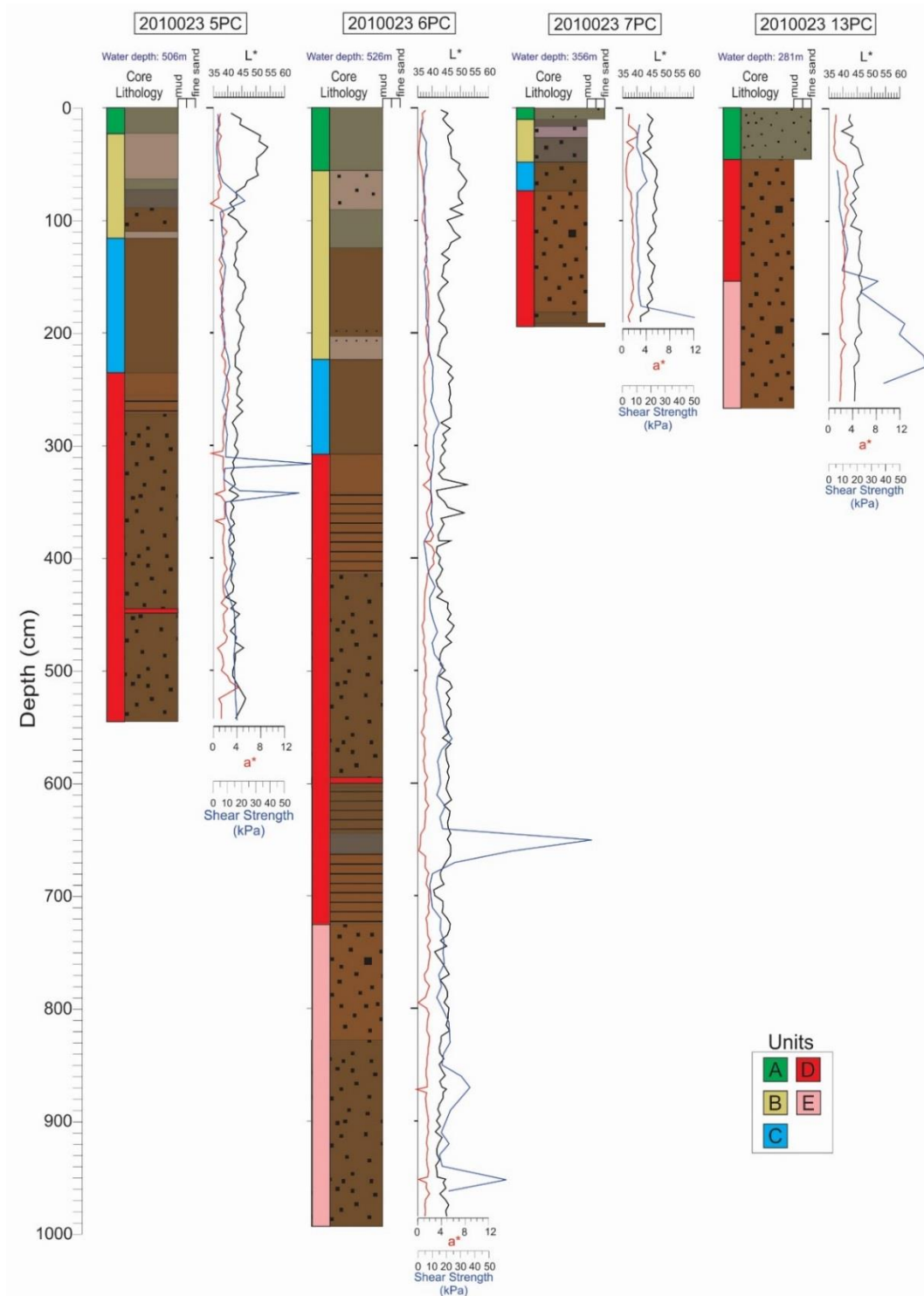


Figure 14c. Downcore summary plot for cores 5, 6, 7 and 13. 13 is included not based on geographic proximity, but on similarity in shear strength.

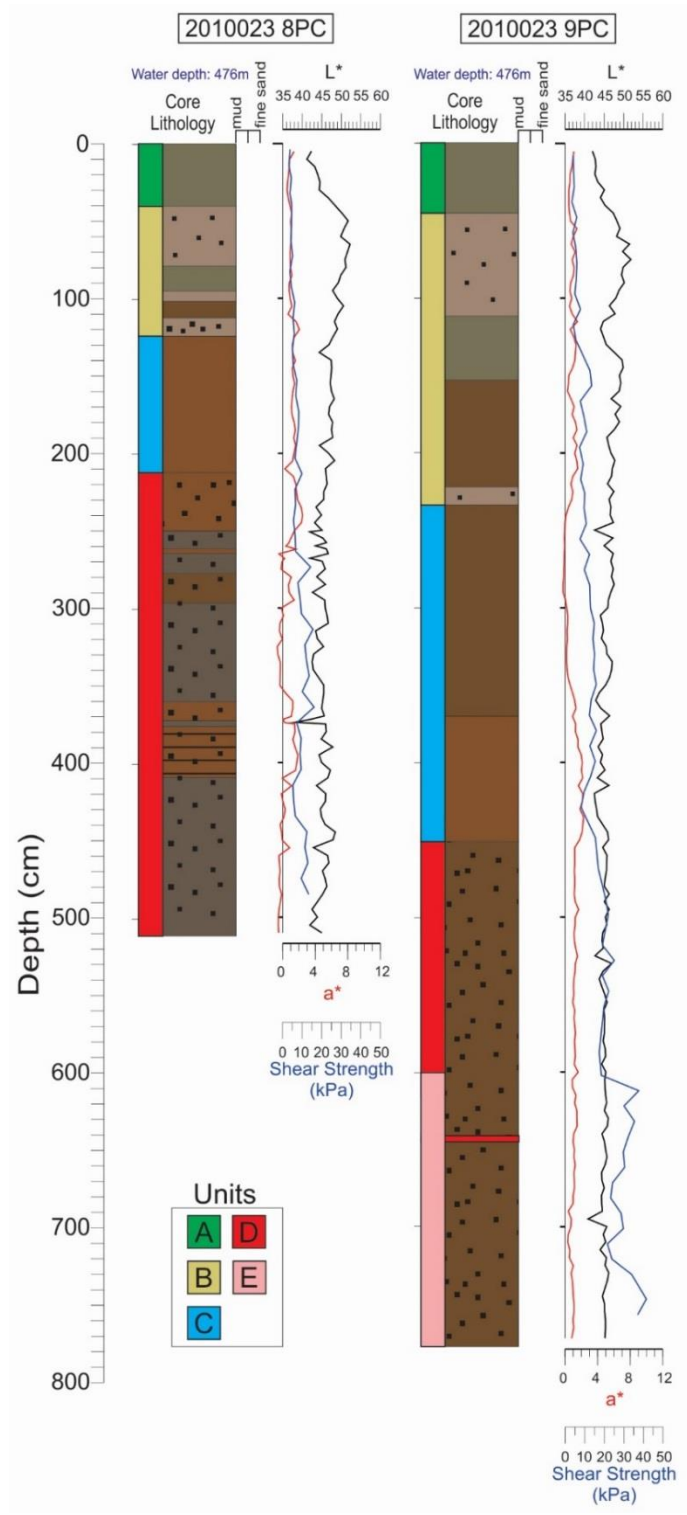


Figure 14d. Downcore summary plot for cores 8 and 9.

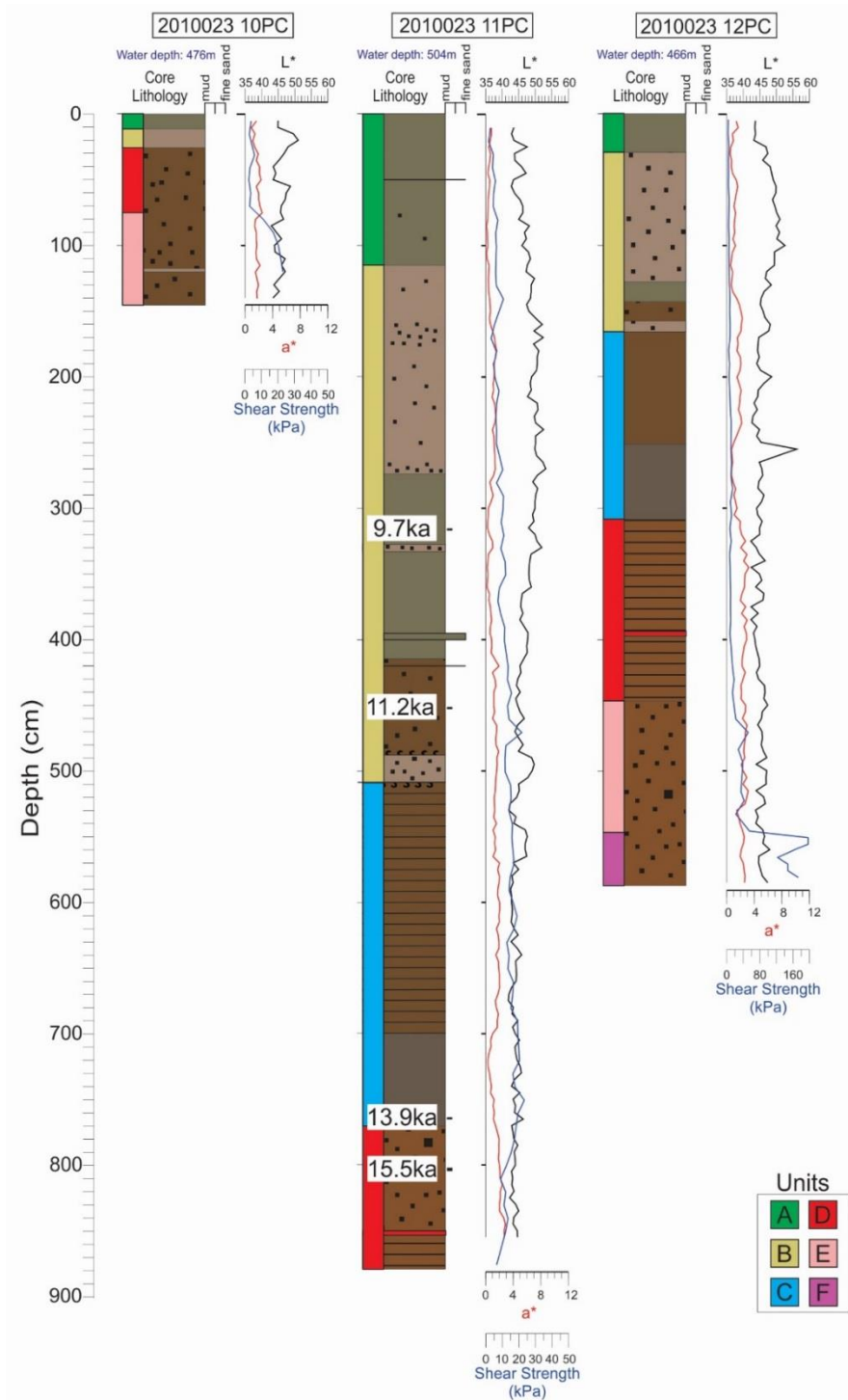


Figure 14e. Downcore summary plot for cores 10, 11 and 12. Note change in scale for shear strength in core 12.

### **4.3.3 Summary of lithostratigraphy**

Units A, B and C are thicker in basins and thin or absent on slopes. Because Units D, E and F tend to be cut off at the bottom of the core, their relative thicknesses cannot be reliably determined. Also, cores 1, 2, 3, 4 and 13 may have undergone substantial erosion during their history, creating an unconformity and eliminating some units. The unit thicknesses show that cores in basins have thicker units than those on highs and cores on slopes are like those of the cores on highs.

## **4.4 Geochemistry of cores**

### **4.4.1 Portable X-Ray fluorescence (pXRF) summary**

Down core XRF plots can be seen in figures 15a – 15e. Ti (ppm) is plotted to show if an element ratio peak is real (eg. Ca/Ti) or an effect of low Ti, as a lower Ti value would cause an artificial peak. Core 11 shows a constant Ti (ppm) until 508 cm, where Ti (ppm) begins to increase downcore until 545 cm, where it remains constant. Cores 2, 3, 8 and 12 also show an overall increase in Ti (ppm) downcore. Core 2 shows dips of two orders of magnitude in Ti (ppm) in the sandy beds near the base of Unit A. Core 3 shows a sharp decrease in Ti (ppm) below 330 cm.

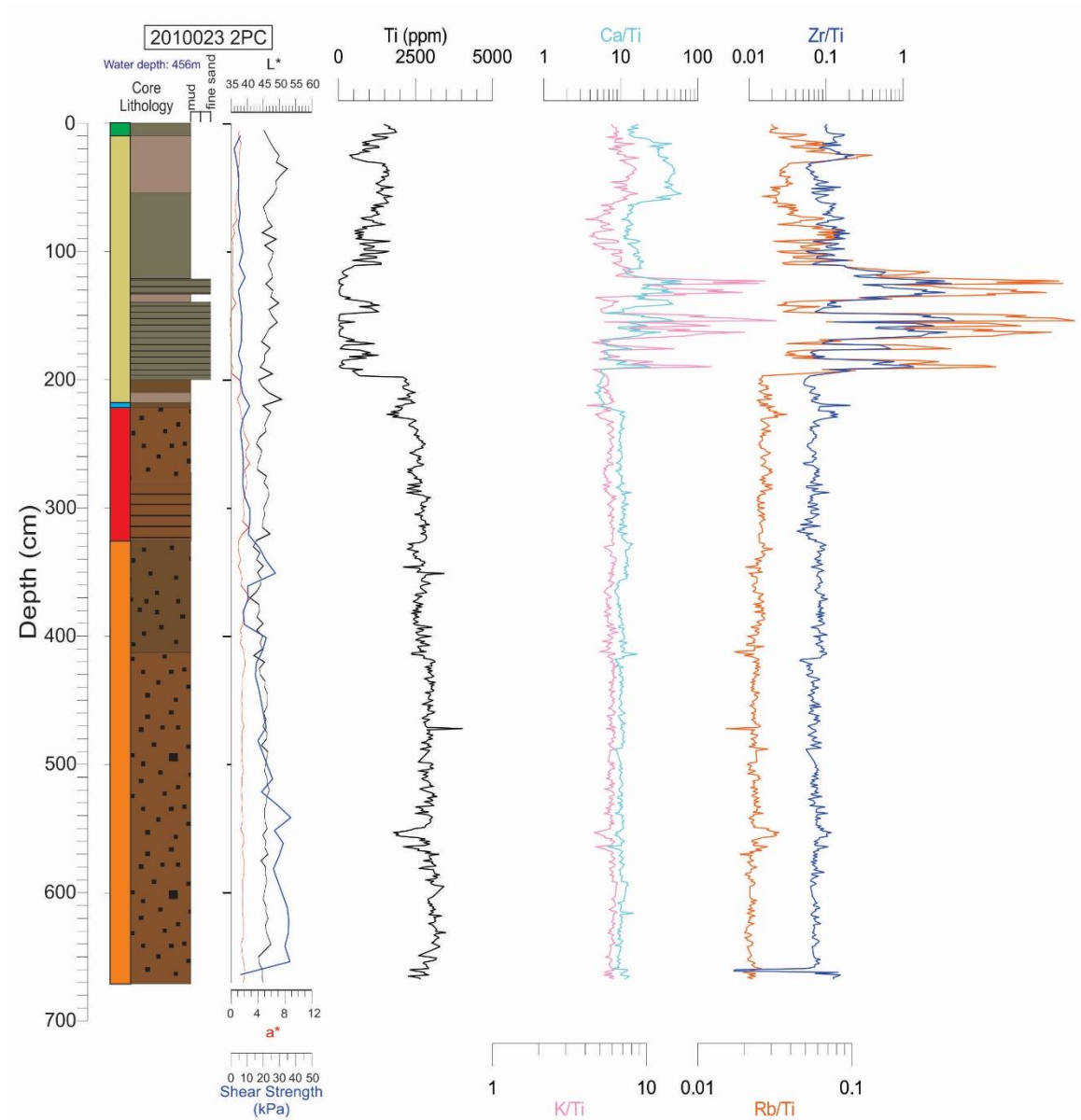


Figure 15a. Downcore XRF of core 2.

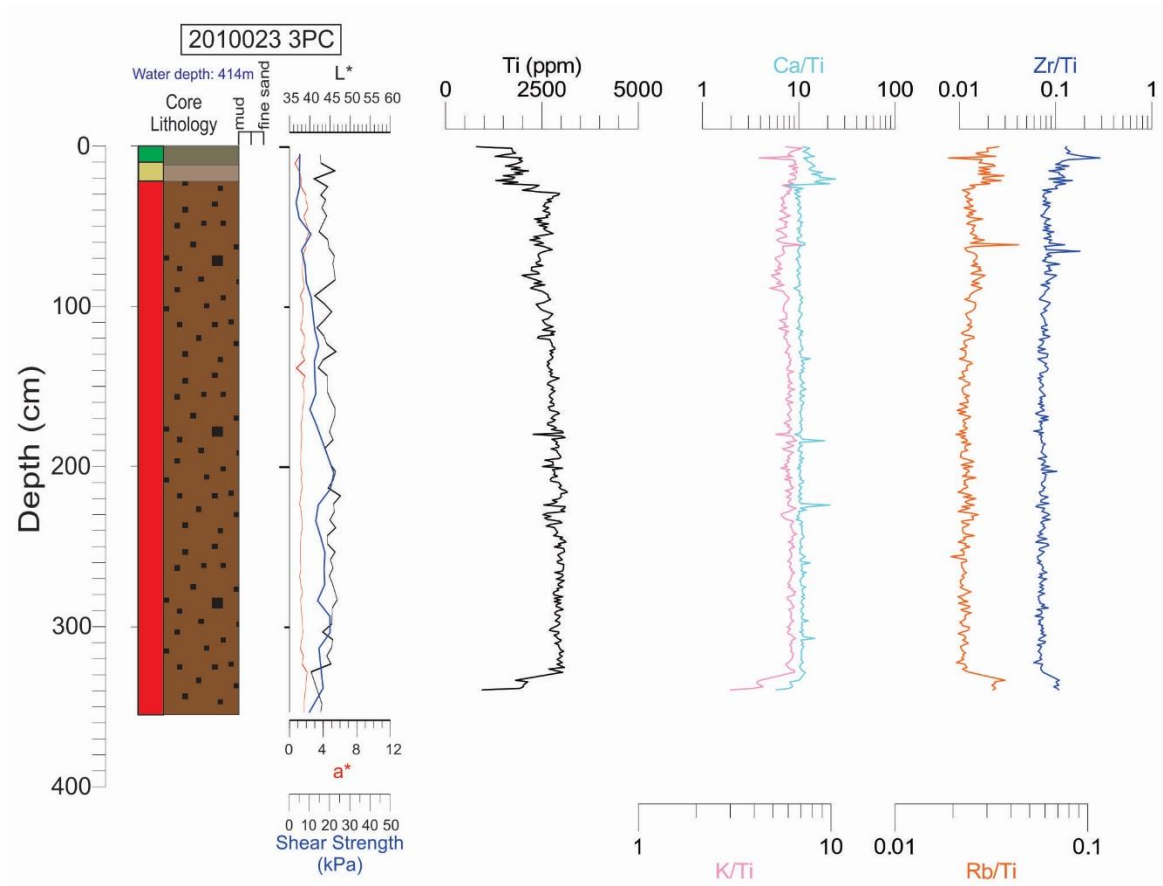


Figure 15b. Downcore XRF of core 3.

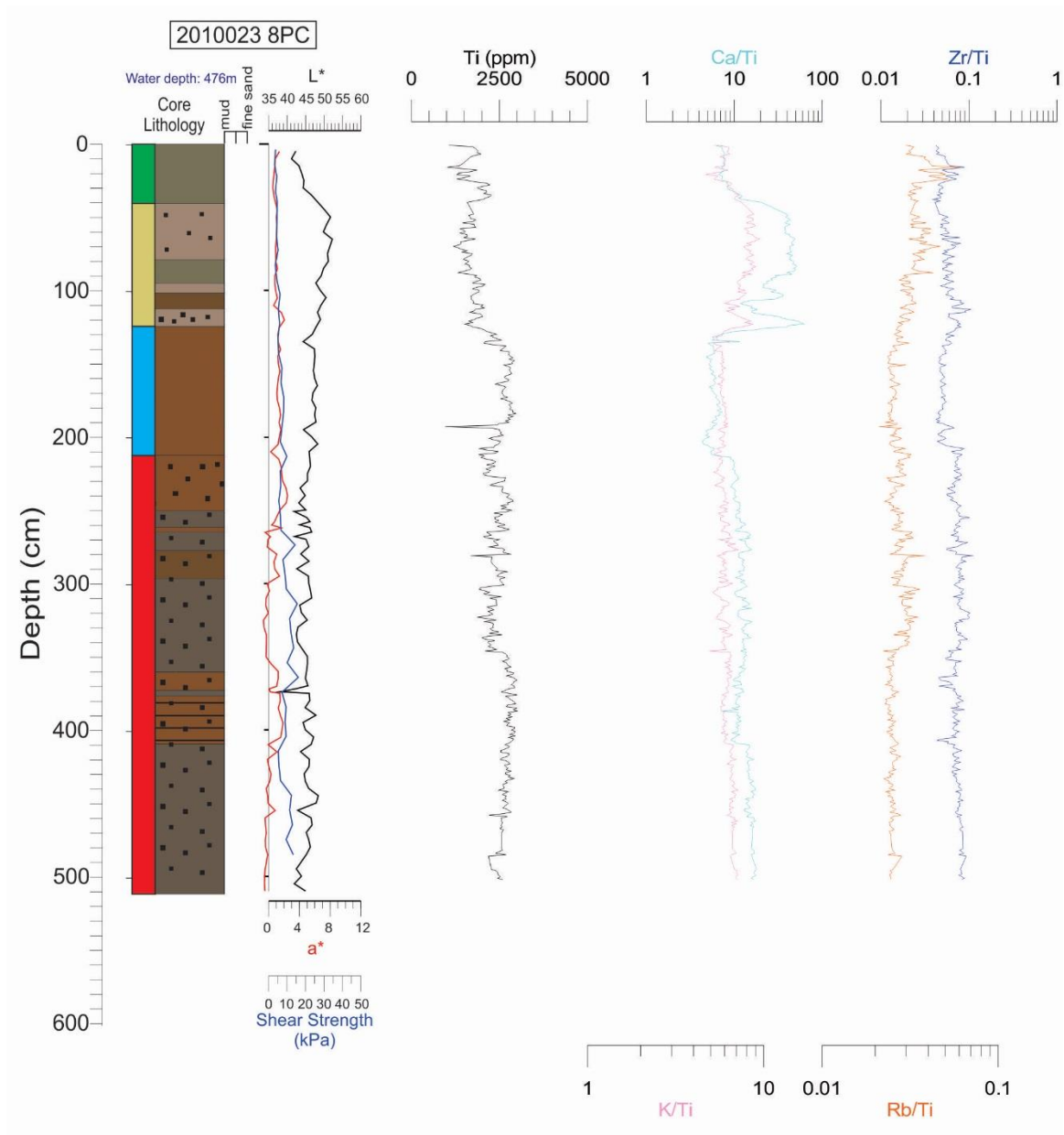


Figure 15c. Downcore XRF of core 8.

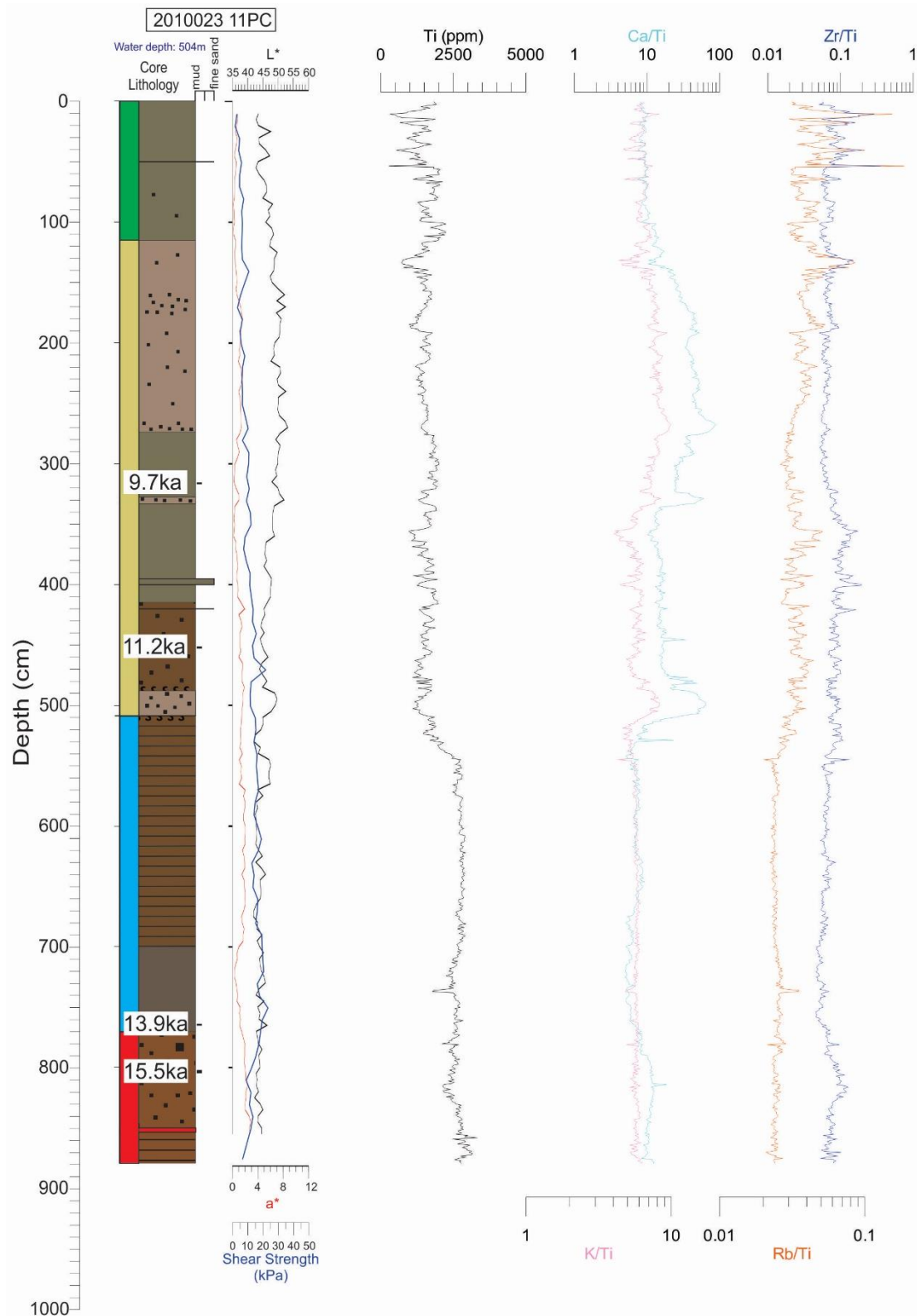


Figure 15d. Downcore XRF of core 11.

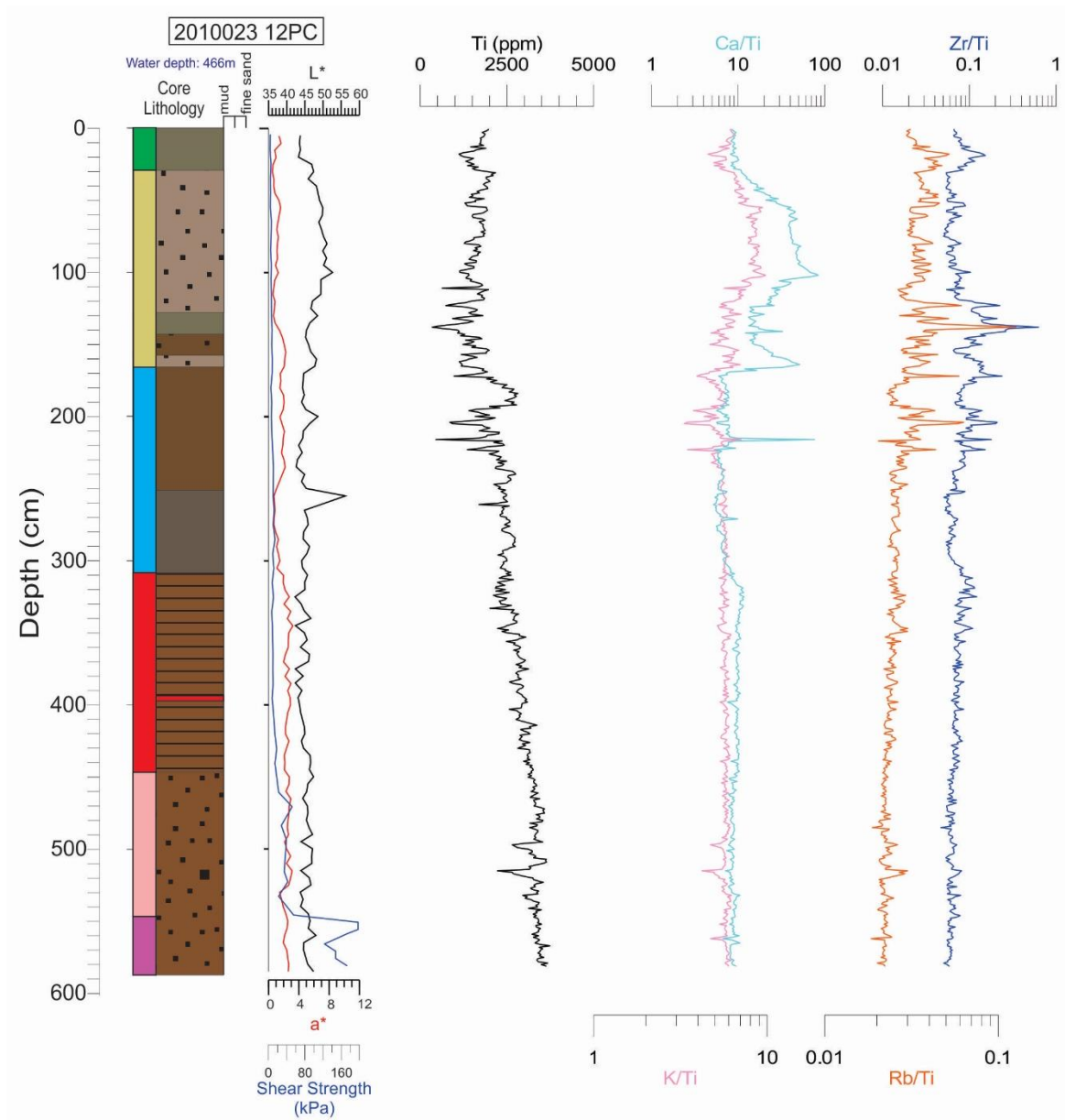


Figure 15e. Downcore XRF of core 12.

Ca/Ti is used as a proxy for carbonate minerals. Unit A has relatively moderate Ca/Ti values of ~10 in most cores with XRF data. Core 8 shows a Ca/Ti value of ~7.5 for Unit A. The tan muds of Unit B show relatively high values of Ca/Ti, reaching values of ~40 to ~50. In core 3 the Ca/Ti for Unit B is ~20. In core 2 Unit B the Ti ppm is three

orders of magnitude lower in the sandy olive grey muds than surrounding muds. The olive grey and brown muds of Unit B show relatively moderate Ca/Ti values of ~10.5. Unit C has relatively low Ca/Ti values in all cores in which it is present, with values typically around 6. Unit D has moderate Ca/Ti values like Unit A, being ~10.

#### **4.4.2 Provenance**

Using geochemistry downcore binary plots were created to compare the changes in sediment source between the units. The cores 2, 11 and 12 are chosen for binary plots. Core 11 was selected as it is the reference core for this study. Cores 2 and 12 were selected as they contain Units E, F and G between them, which are not present in Core 11.

Rb vs K is used to determine whether the source was more mica-rich or feldspar-rich. Values are plotted as Rb ppm vs K<sub>2</sub>O wt% as done in Zhang et al. (2014) to determine whether the source material is mica-rich or feldspar rich. These plots show distinct trends between the units (Fig. 16 a & b). Unit A shows a weak positive trend. Unit B shows a scatter of data points, with an overall weak positive trend. Unit C shows a positive trend, with data points in Unit C plot similarly to the scattered distribution of Unit B. Unit D shows a positive trend with a higher Rb (ppm)/K<sub>2</sub>O (wt%) ratio than unit C. Units E and F show the same positive trend as Unit D, but both with a higher Rb (ppm)/K<sub>2</sub>O (wt%) ratio. Unit G shows a scattered distribution with a high Rb (ppm)/K<sub>2</sub>O (wt%) ratio.

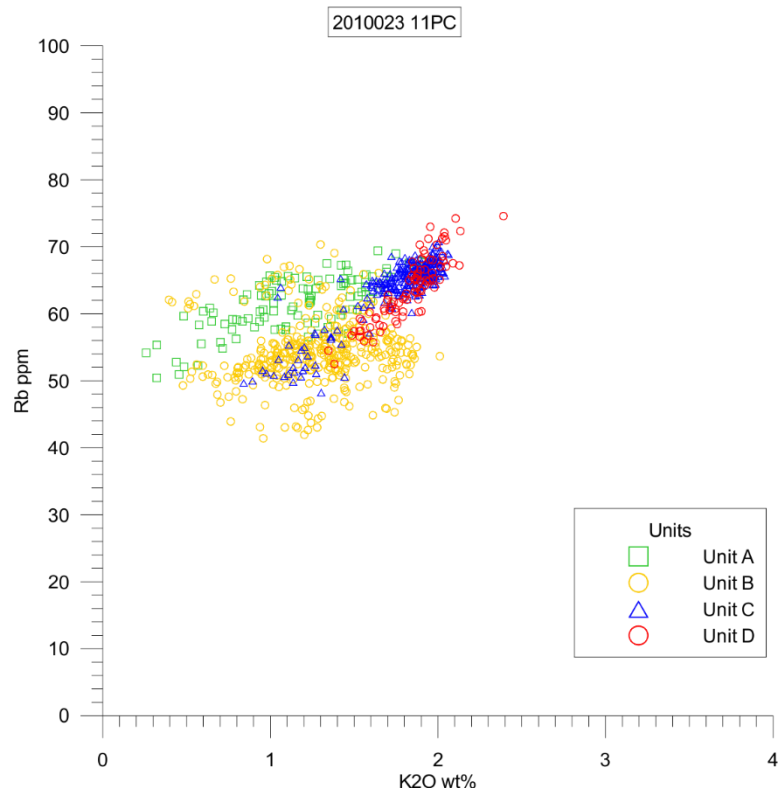
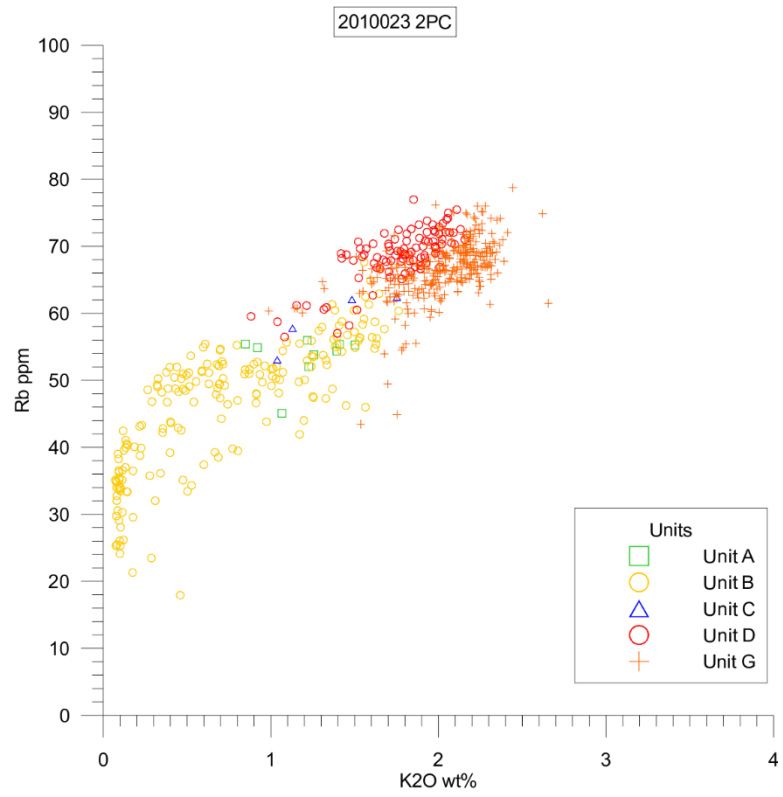


Figure 16a. Rb vs  $K_2O$  for cores 2 and 11.

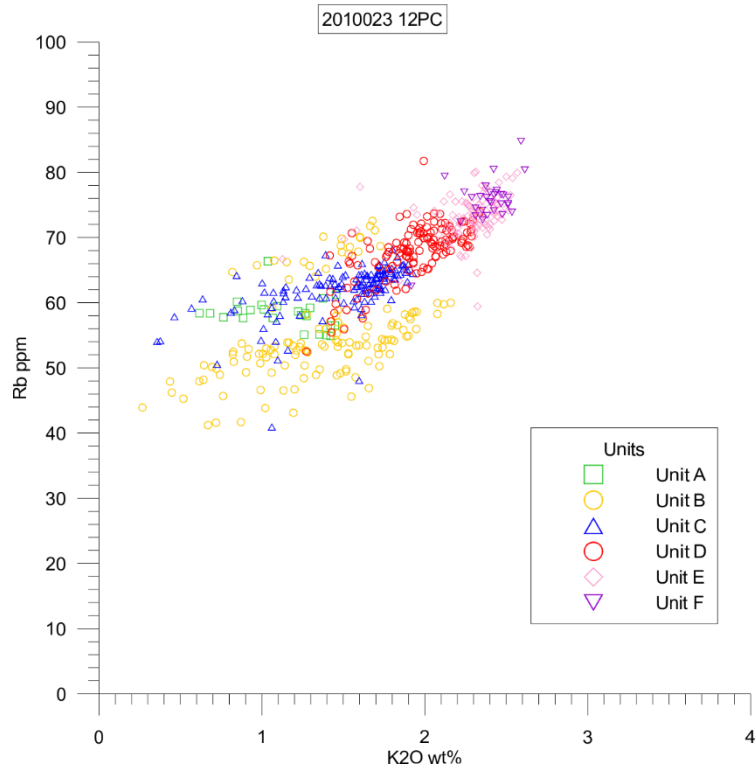


Figure 16b. Rb vs K<sub>2</sub>O for core 12.

Zr vs Ti is used as a proxy for sand, as higher silt and sand content correlates with Zr increase and Ti decrease. Unit A in Core 12 shows a negative trend in Zr vs Ti, whereas the nearby core 11, which is located in a basin, shows a flat-lying trend (Fig. 17b). Bulk density data for core 11 shows an average of 1.824 mg/m<sup>3</sup> and in core 12 an average of 1.859 mg/m<sup>3</sup>. This bulk density suggests that core 12 may have a higher abundance of sand and silt compared to clays, but grainsize data are needed to prove this. Unit B shows a scattered distribution, with the majority of the data lying in the low Zr range. Unit C shows a scattered distribution with most data points lying in the high Ti range, and some data points with distribution similar to that of Unit B. Unit D shows a weak negative trend with high values of both Zr and Ti. Units E and F show scattered

distributions with Ti values that are ~500 ppm greater than those of Unit D (Fig. 17a).

Unit G shows a scattered distribution with lower Ti ppm than Units E and F (Fig. 17a).

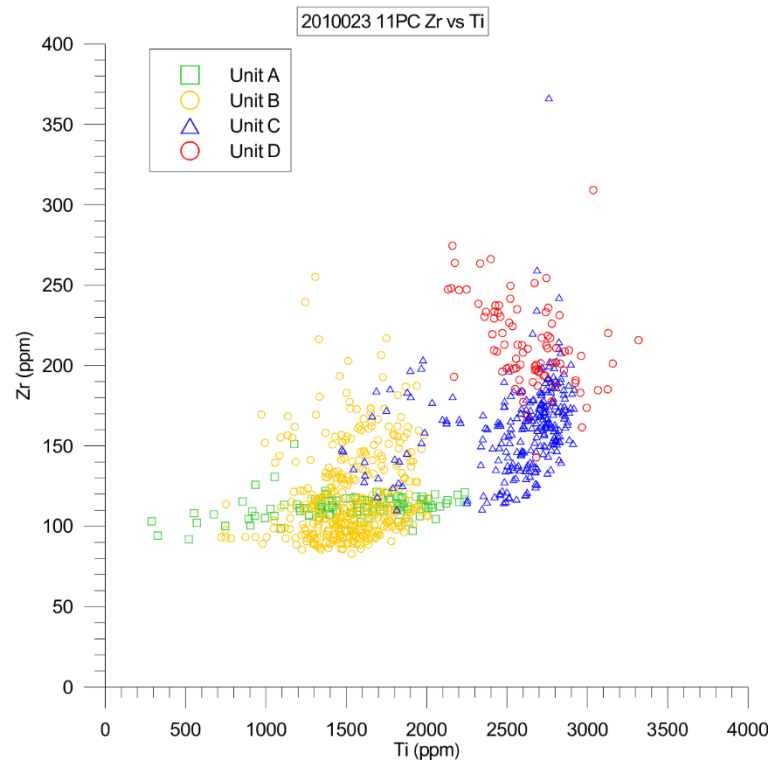
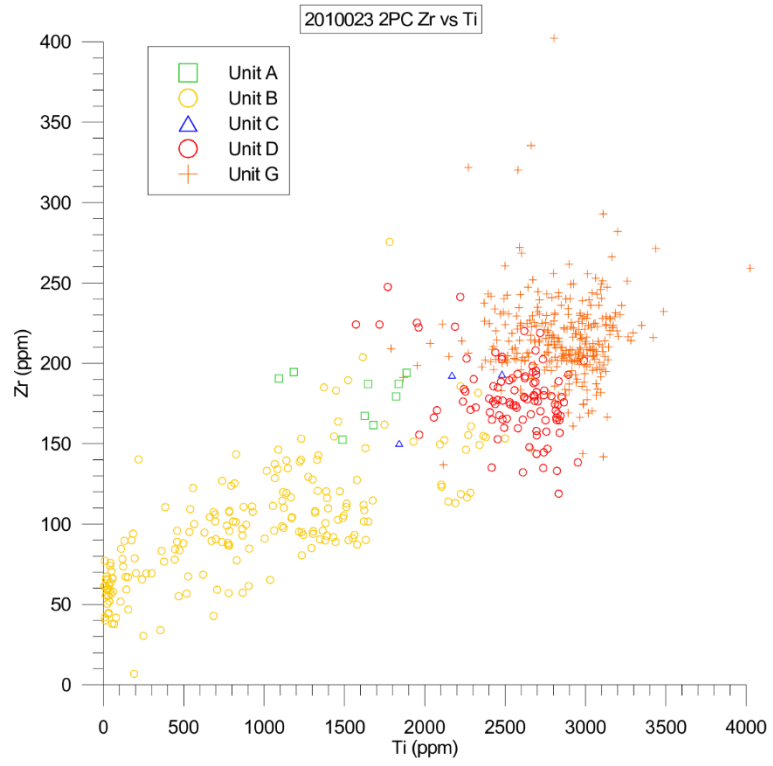


Figure 17a. Zr vs Ti plots for cores 2 and 11.

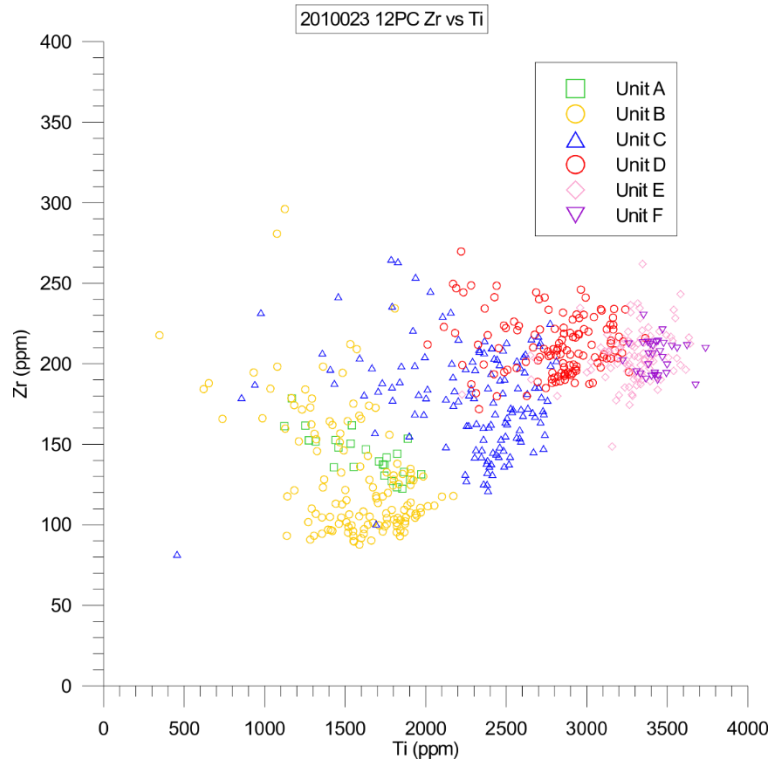


Figure 17b. Zr vs Ti for core 12.

Sr vs Ca was also plotted to compare the variation in sediment source between units. Unit A shows a positive trend (Fig. 18). Unit B shows a positive trend with Ca values exceeding 100000 ppm. This very high Ca values in Unit B is likely due to an abundance of carbonate minerals present in Heinrich layers. Unit C shows a positive Sr vs Ca trend, but with higher Ca values than Unit A. Unit D shows a positive trend. Unit E shows a scattered distribution with a lower Sr than that of Units D and F. Unit F shows a positive trend with higher Sr and Ca values than Unit D.

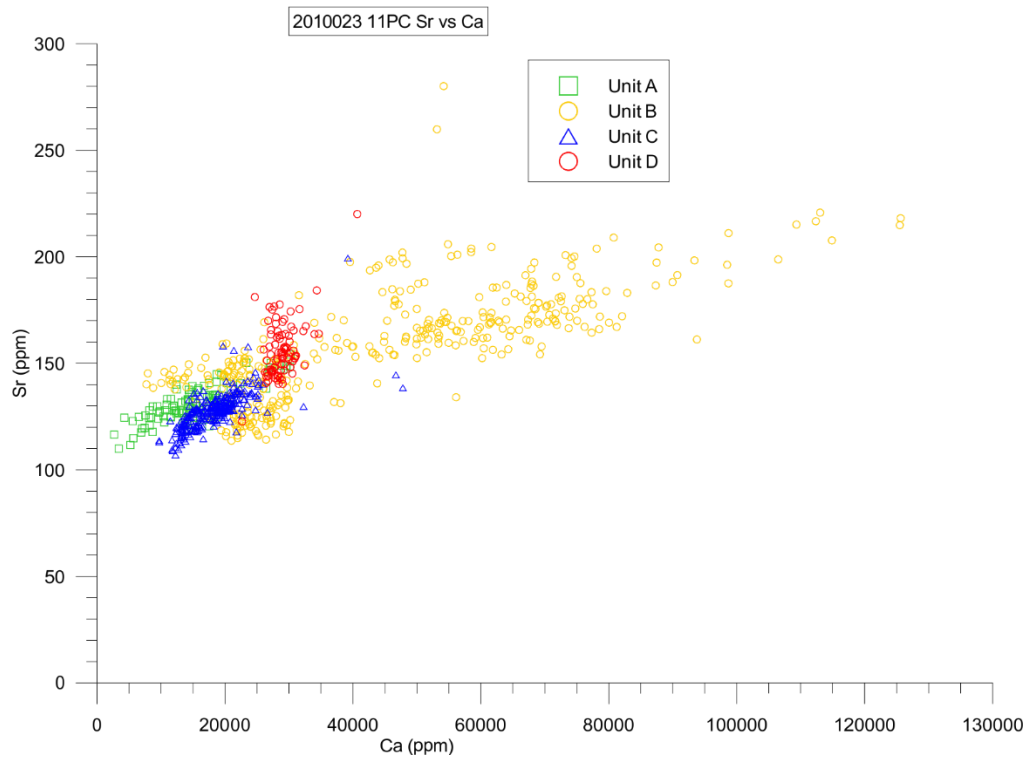
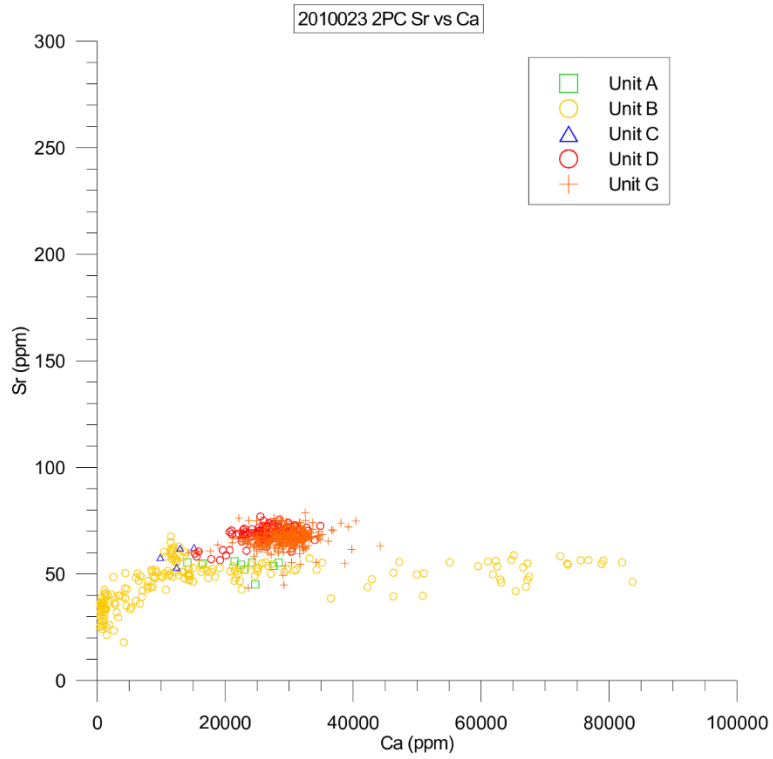


Figure 18a. Sr vs Ca for cores 2 and 11.

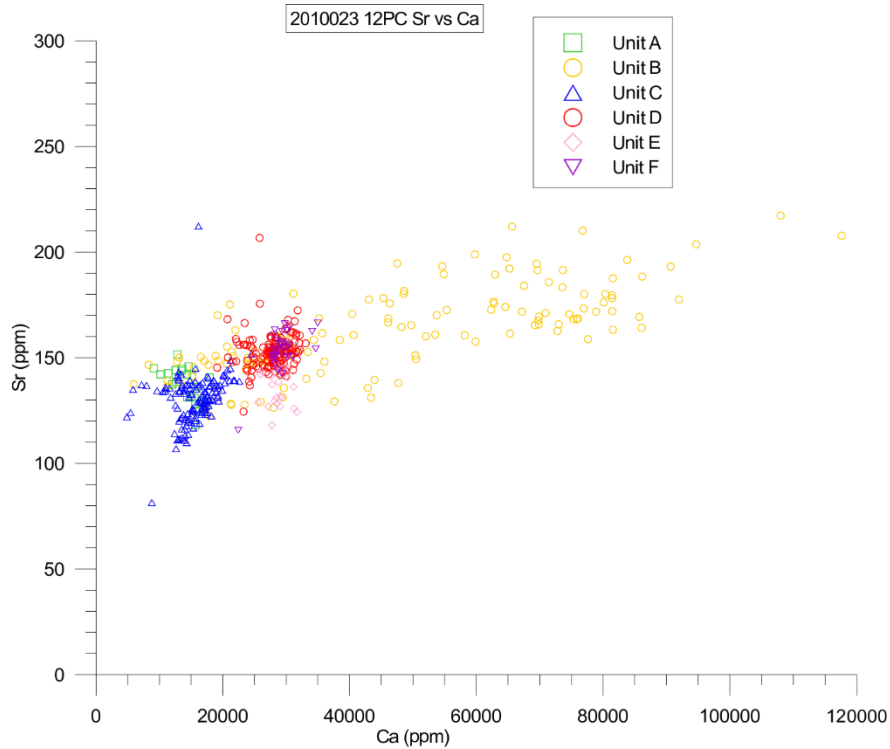


Figure 18b. Sr vs Ca for cores 2 and 11.

## 4.5 Colour

### 4.5.1 Lightness $L^*$

The  $L^*$  for all cores can be seen in Figures 14 b – e.  $L^*$  shows a gradual increase downcore from ~43 in Unit A until it peaks near the middle of Unit B (270 cm in core 11). After this peak in Unit B,  $L^*$  gradually decreases until the beige mud at the base of Unit B, where the  $L^*$  spikes to 54 (487 to 508 cm in core 11). After this spike the  $L^*$  drops again to 42 before peaking to 47.5 near the top of Unit C (545 to 565 cm in core 11). The  $L^*$  is then relatively constant at ~44 until the end of core 11.

#### **4.5.2 Redness a\***

The downcore a\* can be seen for all cores in Figures 14 b – e. Unit A has an a\* of ~0.5 and decreases downcore. Unit B shows an increase in a\* to ~1.5 in beige muds and a decrease to ~0.5 in olive grey muds. Unit C shows a relatively higher a\*, the top of Unit C shows a\* of ~1, with a sharp increase to ~2 at 565 cm in core 11. The a\* of Unit C decreases at the bottom in grey muds. Units D, E and F have an overall higher a\*, with values ranging from 1 to 3. Unit D in core 8 has much lower a\*, reaching negative values, this is likely due to its high content of grey muds. Unit E in core 4 has an a\* that is relatively constant around 1. This low a\* coupled with brown mud in Unit E of core 4 suggests that it is different from Unit E in the other cores.

#### **4.6 C-14 dating**

Mollusc shells were sampled from core 11 for carbon-14 dating. The shells selected were intact in order to minimize the possibility that the shell had been transported. This is because if the shell had been mobilized it may yield a much older age than the sediments it was sampled from. The shell from 316-317 cm was selected for dating some of the events in Unit B. The shell from 451.5-452.5 cm was selected to get an approximate date on a Ca/Ti peak at 487 to 508 cm. The shells at 763-764 cm and 802-804 cm were selected to attempt to date the boundary between Unit C and Unit D.

Table 2. Radiocarbon dates for core 11.

Core	Depth (cm)	Conventional C-14 age (yr)	Calibrated age (sigma 1 age range) (cal yr BP)
2010023 0011 PC	316-317	9195 ± 20	9746 ± 80.5
2010023 0011 PC	451.5-452.5	10380 ± 25	11222 ± 49
2010023 0011 PC	763-764	12615 ± 25	13953 ± 74.5
2010023 0011 PC	802-804	13495 ± 25	15470 ± 116.5

The conventional radiocarbon date was calibrated using the Calib 7.1 program (Stuiver & Reimer, 1993) using the MARINE 13 calibration dataset (Reimer et al., 2013). This calibration was done to correct for variations in C-14 production and the Marine Reservoir effect. The local reservoir correction ( $\Delta R$ ) used was  $144 \pm 38$  from Li and Piper (2015), as the study area is also subject to the Labrador current. All references to C-14 dates in the text are in calibrated ages.

## 5. Discussion

### 5.1 Interpretation of seismic units and facies

Units 1 and 2 (Fig. 19) occurs in Cenozoic flat lying sediment and is truncated by younger erosion. This erosion includes the formation of the Middle Mound (Fig. 8 k-l) and a small erosional channel to the north (Fig. 8 o-p). Based on these cross-cutting relations, these Units are older than the nearby glaciotectionic events. Seismic facies 1 of these units is interpreted to be till and as such to have formed from a previous glacier which was grounded on the continental shelf some time during the Pleistocene. As sea levels rose during the Pleistocene, this glacier began to float at its edges first, which

allowed for glacial till to begin dropping out of the base of the ice as it melted. This till then formed small till deltas, which primarily dip in the direction the ice first started lifting, which are seen in Figure 7 (d-e). Seismic facies 1 occurs twice above the Notre Dame Unconformity as visible on the bank to the north. These repetitions show that glacial advances have occurred at least twice in the seismic record. Facies 1 does not occur in the basins of the NDT. This is consistent with Shaw and Longva (2017) as they suggest the ice was fast flowing and fast flowing ice leaves little till. Therefore, when the Northern Basin was carved by ice and the Middle Mound was formed, the ice moved quickly.

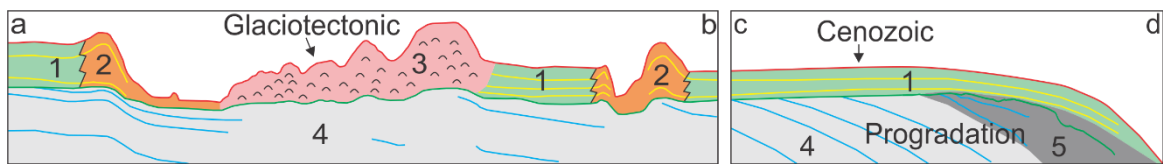


Figure 19. Summary of seismic units with notes on interpretation. The area labelled progradation occurs above the pre-glacial shelf.

Unit 1 grades into Unit 2 where facies 1 begins to show wedging. This wedging occurs below the berms pointed out by Shaw et al (2011) and Shaw and Longva (2017). This may be due to shortening from compression caused by the ice which caused the glaciotectonism.

Unit 3 (Fig. 19) occurs as the Middle Mound and is interpreted like that in Shaw et al. (2011) and Shaw and Longva (2017). This incoherent seismic reflection is due to the mobilization of sediments. As the ice plowed through the sediments it pushed them into other flat-lying sediments, creating a fault where incoherent seismic reflectors is present laterally to flat-lying reflectors.

Units 4 and 5 (Fig. 19) occur below the Notre Dame Unconformity. These units are of an unknown age and the unconformity which truncates them represents a glaciation of unknown age. Facies 3 which forms these units is interpreted to have formed as a major glacier progressed towards the continental slope. Unit 4 formed first as this glacier deposited proglacial till deltas on top of the previous continental shelf. Each time the glacier made a major advance, the previous till delta became covered by new till, causing the deltas to truncate the top of the previous one (Fig. 9). Once the glacier reached the slope, Unit 5 began to form and the steeper angle allowed for better preservation of clinoforms (Fig. 9).

## **5.2 Glaciotectonics**

From air-gun seismic profiles, there is a surface interpreted as a glide plane between the incoherent seismic of the Middle Mound and horizontal flat-lying reflectors (Fig. 20). The glide plane truncates these flat-lying reflectors horizontally positioned to it in a step like pattern which dips toward the Middle Mound. Flat-lying reflectors below the truncated flat-lying reflectors are continuous below the incoherent Middle Mound. This glide plane is interpreted to be a thrust, which is consistent with Shaw et al (2011) and Shaw and Longva (2017) interpretation of the Middle Mound having been formed due to glaciotectonism. If the sediment was bulldozed by a glacier and pushed through other sediment it should leave the underlying sediment relatively undisturbed and cut through sediments horizontally.

The mound at the east end of the South Trough also shows flat-lying seismic reflectors below the incoherent facies. However, the orientation of the profile reveals no

further information. It is possible this formation also has a glide plane, however to see this would likely require a seismic profile perpendicular to the profile which intersects it. As this mound shows incoherent seismic overlying flat-lying reflectors it is also likely to have been formed due to glaciotectonism.

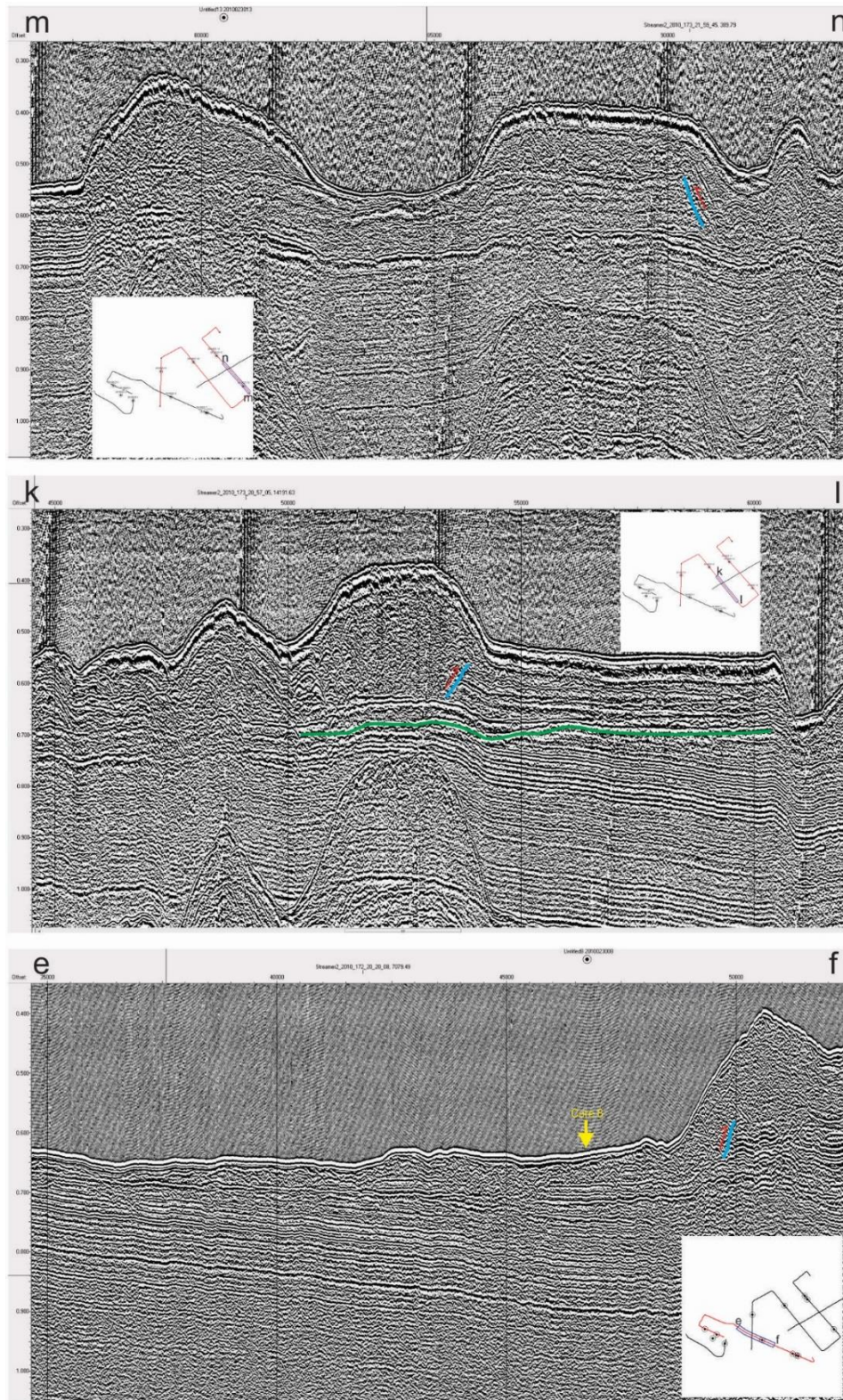


Figure 20. Air-gun seismic profiles showing glide planes, in blue, through the Middle Mound, direction of inferred movement as a red arrow.

The timing of this glaciotectonic event can not be accurately determined with available information. This event is unlikely to be older than the Wisconsinan. However, flat-lying reflectors between the Notre Dame Unconformity and the incoherent seismic of the Middle Mound shows the event forming the Middle Mound is younger than the regional unconformity. Based on sediment depths and the carbon-14 dates in core 11, the suggestion of Shaw and Longva (2017) that this glaciotectonism occurred during the Late Wisconsinan, 30 ka, is not unreasonable. The berms within the Northern Basin show flat-lying seismic reflectors which suggest that they were not tectonised like the sediment beside them (Fig. 21, showing seismic e-f, h-I, n-o).

From the available seismic data the interpretation of glaciotectonism of Shaw and Longva (2017) is correct. This would mean the North Basin is a decollement surface as interpreted by Shaw and Longva (2017). The ice which caused this glaciotectonism was also fast-flowing as suggested by Shaw and Longva (2017) as there is little till in the North Basin. The direction of ice flow through the trough is possibly like that suggested by Shaw and Longva (2017). Consistent with this is a lack of a berm on the North Ridge near the slump block. The berm may have been bulldozed (Fig. 22). However, the berms in the North Basin are parallel with the trend of the NDT. As these berms contain flat-lying reflectors, showing they are undisturbed (Fig. 21), the ice which flowed through the trough was flowing parallel with the trough. The ice may have then entered the trough from a more westerly direction rather than from the north-west (Fig. 22).

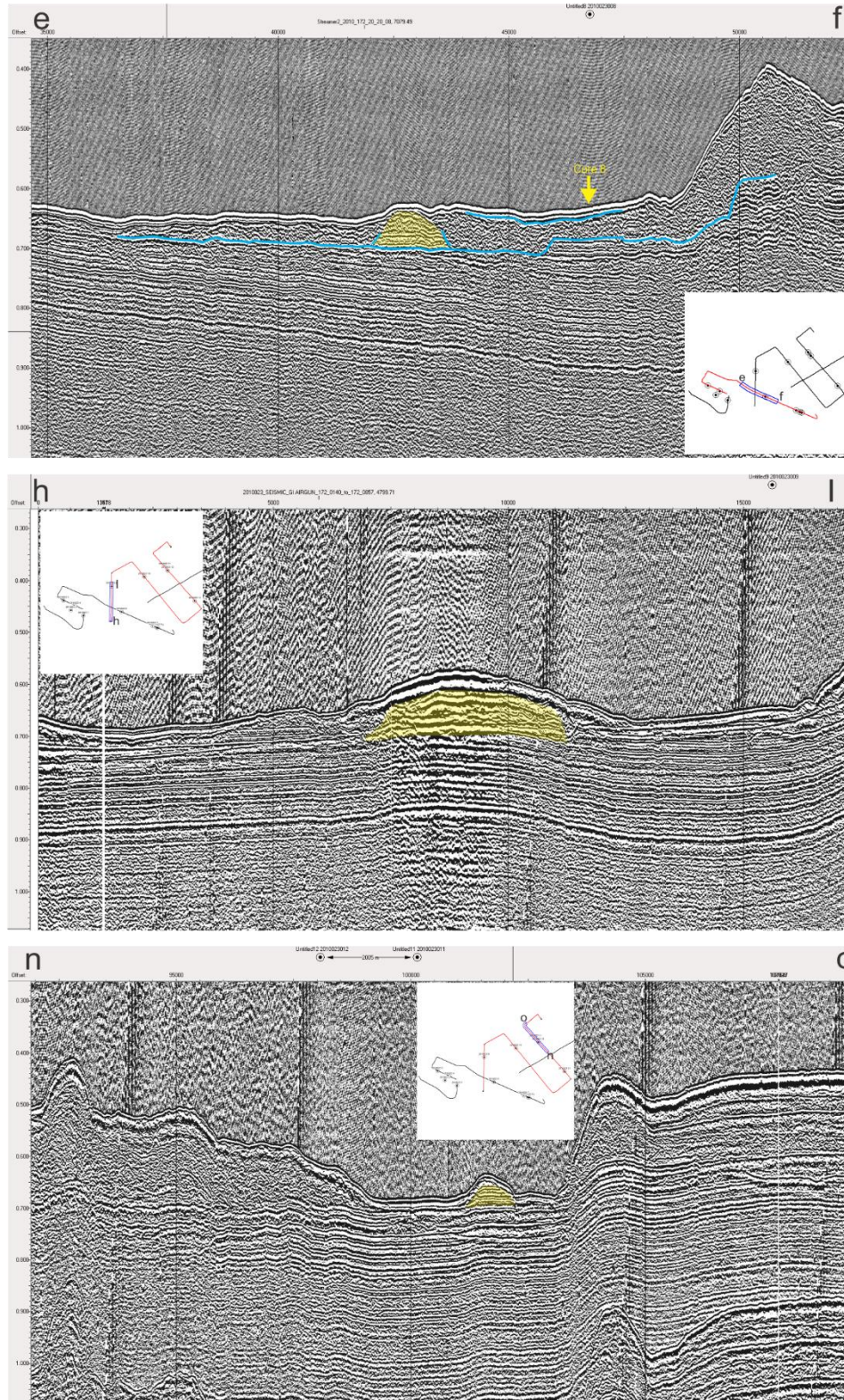


Figure 21. Air-gun profiles in the North Basin showing berms with truncated flat-lying reflectors, highlighted in yellow.

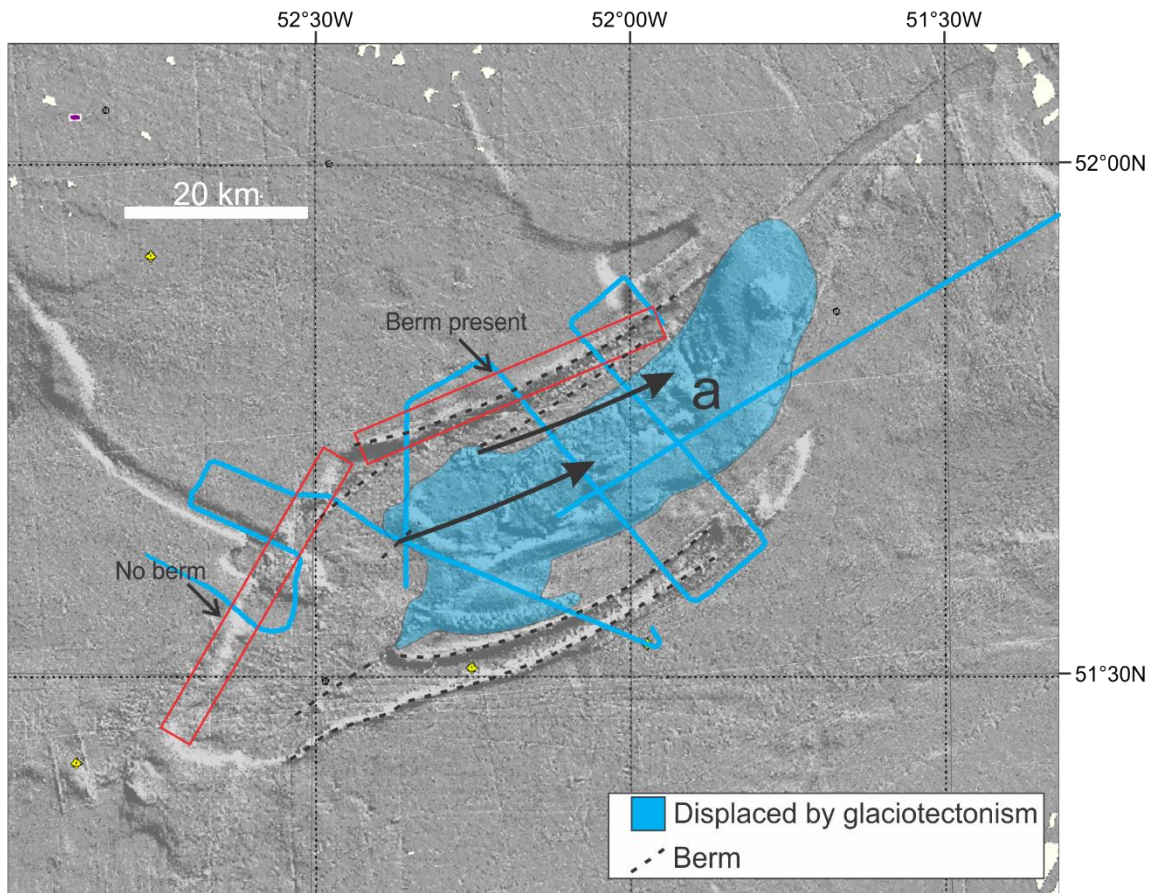


Figure 22. Seismic based interpretation of glaciotectionism of the Middle Mound. Blue lines depict seismic profiles. Also shows where the berm is and is not present along the North Ridge.

### 5.3 Correlation of cores and age model

The cores which are taken from slopes and highs overall have thinner units than those which are taken from basins. Unit A is present in all cores and is easily correlated between cores. Unit B is present in most cores, though in some is present as a thin tan mud bed. Thin or absent Unit B occurs in short cores. Cores where Unit B is short are 3, 7 and 10; cores where Unit B is absent are 1, 4 and 13. From 3.5 kHz it can be noted the cores with thin or absent Unit B's are those without distinctive mud layers, whereas cores with longer a Unit B are taken from where there are distinct mud layers. Unit C is absent

in cores 1, 3, 4 and 10 and thin in core 2. With the exception of core 10, which on a berm, these cores that are lacking Unit C are present on or around the slump block on the southwest side of NDT. With the exception of cores 11 and 12, none of the other core with Unit C have grey mud at the base. Unit D is present in all cores, and cores 1, 5, 6, 9, 11 and 12 contain a bright red mud, which is interpreted to be a correlatable horizon. Units E, F and G are not present in core 11, and all occur below Unit D. The high shear strengths of these units may be due to having originally been buried deeper or due to ice grounded on the sea floor, compacting the sediment.

Correlations were made between the pXRF data of Ca/Ti in core 11 of this study and carbonate wt% in Jennings et al. (2015) and Ca/Ti in Li and Piper (2015) in cores respectively farther north and farther south beneath the Labrador Current (Fig. 23). The calibrated carbon-14 date in core 11 at 451.5 – 452.5 cm giving a 11.2 ka date allows for the correlation of the Ca/Ti peak from 487-508 cm to be correlated with Heinrich Layer 0 recognised in Li & Piper (2015) and in Jennings et al. (2015). This 11.2 ka date also allows this carbonate peak to be correlated with Heinrich Layer 0 in Flemish Pass from Li & Piper (2015). The carbonate peak from 326-333 cm in core 11 correlates with the Gold Cove retreat at 10.6 ka found in Cartwright Saddle by Jennings et al. (2015). Peaks above this in the pXRF data are somewhat masked due to the overall high carbonate abundance through the tan layer of Unit B from 115-274 cm. Correlating the peaks from this interval places 287-294 cm in core 11 at 9.7 ka during the Noble Inlet advance (Jennings et al. 2015), 265-274 cm at ~9.4 ka with no specified event, 230-241 cm during the Noble Inlet retreat at 9.1 ka, 190-192 cm with the Early opening of the Tyrell Sea at 8.5 ka, and 123-129 cm at ~8.2 ka, the Final Lake Agassiz Flood (Fig. 33).

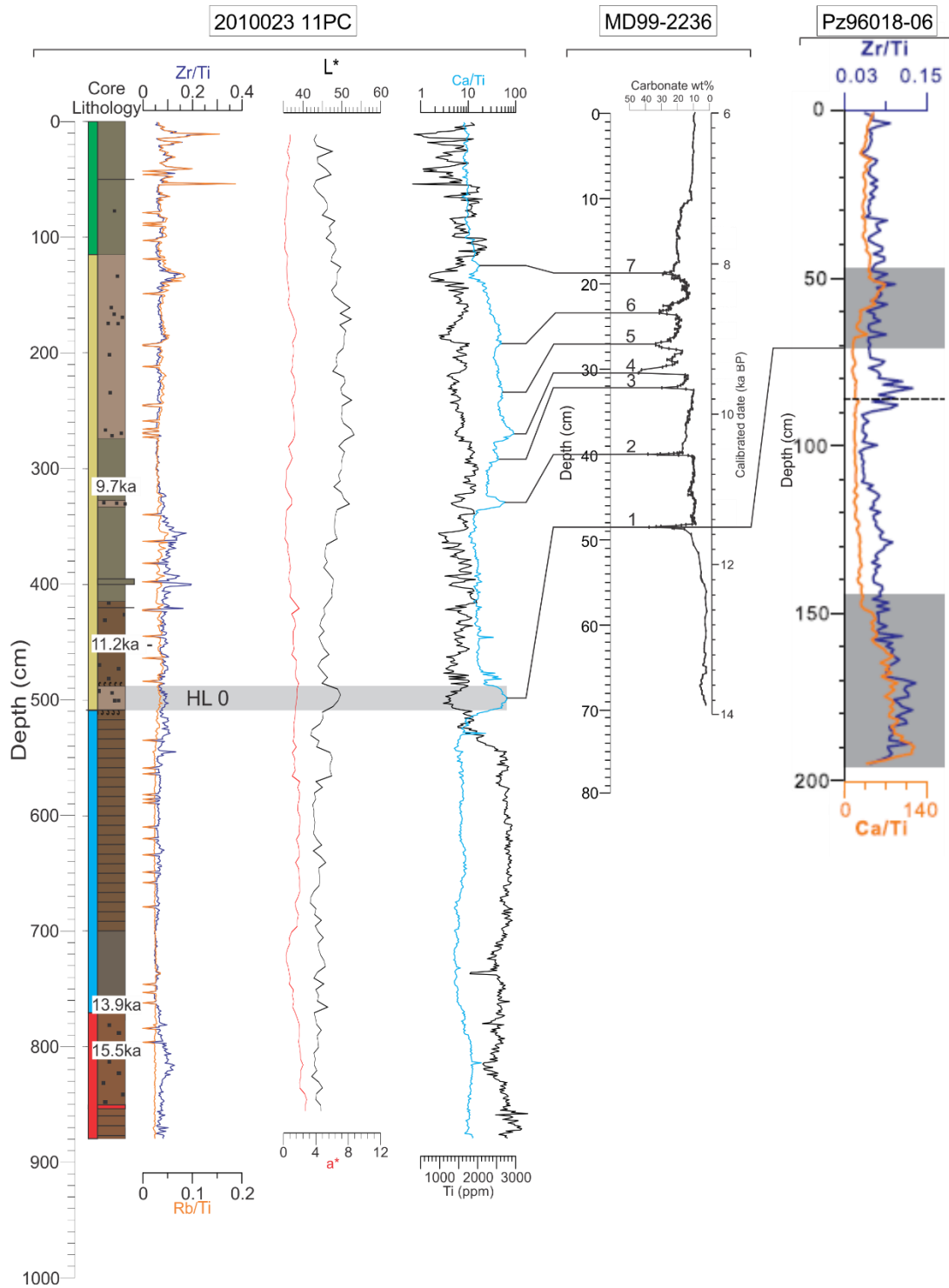


Figure 23. Plot of Ca/Ti and Zr/Ti in core 11 comparing with core MD99-2236 from Cartwright Saddle (Jennings et al. 2015), showing similar peaks in Ca/Ti and Ca wt% at similar ages. Also comparing H0 with core Pz96018-06 from Flemish Pass (Li & Piper, 2015). The correlated events with Cartwright Saddle are as follows: 1) Heinrich Event 0 at 11.7 ka; 2) Gold Cove retreat at 10.6 ka; 3) Noble Inlet advance at 9.7 ka; 4) 9.4 ka with no specified event; 5) Noble Inlet

retreat at 9.1 ka; 6) Early opening of the Tyrell Sea at 8.5 ka; 7) Final Lake Agassiz Flood at 8.3 ka. Modified from Jennings et al. (2015) and Li & Piper (2015).

#### **5.4 Pre-deglacial history**

Unit G may hold the oldest stratigraphy as it is unique to core 2. This core is taken from the decollement surface from which the slump block slid. It is possible that the piston core was able to penetrate through the muds which deposited over top of this surface and cut into the older sediment. In this event, the boundary between Unit D and Unit G is unconformable. A large time gap between Unit G and Units F, E and D is then possible, however this study has no dates in Unit G to verify this hypothesis.

Units E and F in core 12 shed some light in hypothesizing events which may have occurred prior to Unit D. Each of these units show a sharp increase in shear strength. The sharp increase of shear strength in Unit may be caused by an unconformity, as the sediments may have originally been much deeper, or it may be from ice grounding when the ice was much thicker.

If the top of Unit F is an unconformity, it is possible that Unit E has an increased shear strength due to ice grounding. This would also be consistent with current water depths, as the cores with Units E are typically in lower water depth relative to the cores which lack Unit E. An exception to this is core 6, which is the deepest core (526 m water depth), but shows a gradual increase in shear strength throughout the core to 20 kPa. This gradual increase of shear strength in core 6 is possibly from sediment compaction. It is also possible that these increases in shear strength of Units E and F are both due to ice grounding, or an artifact of an unconformity.

## 5.5 Deglacial history

The sedimentary record of the cores helps reveal the events which occurred during their glacial history. Using Units D and C in core 11 the deglacial history can be described. The base of Unit D in core 11 begins at some time before 15.5 ka. Unit D is sourced from ice-streams which travelled from Notre Dame Bay through the Notre Dame Channel to eventually Notre Dame Trough before reaching the shelf edge (Shaw and Longva 2017). This ice brought IRD and sediments of the St. Anthony basin red beds, giving Unit D its red muds. Some black mud beds are noted at the base of core 11, but with the current information it is uncertain what their source is.

A more concentrated amount of red sediment was transported into the NDT, leaving a bright red mud in Unit D, present from 852-853 cm in core 11. It is possible this increased transport of red sediment may be due to a moraine flooding event like that described by Cameron and King (2011). If a glacier was temporarily static behind its moraine, the sub-glacial hydraulic pressure may allow the build up a subglacial pool of fresh water (Fig. 24) (Cameron and King, 2011). If the glacier were then to retreat or lift off the moraine, any hydraulic head from the weight of the glacier and crevasses of melt water would force the pool of water to flood into the ocean. Any turbulence from this would carry the fine grained sediments which accumulated in the sub-glacial lake. This glacial retreat event may correspond to the calibrated 17 ka ice margin to retreat into fjords on the northeast coast of Newfoundland (Shaw et al. 2006). This would place this bright red mud event around the Heinrich 1 (H1) event, ~15-17.5 cal ka BP, described in nearby Flemish Pass by Li and Piper (2015). This might mean that the carbonate rich H1 event is not present on the Northeast Newfoundland Shelf. The meltwater from Hudson Strait which allowed large quantities of carbonate to be carried and deposited by the

Labrador Current would have been pushed seaward by the meltwaters flowing across the Northeast Newfoundland Shelf. This would make this bright red mud the H1 melting event of the Northeast Newfoundland Shelf. IRD continued to be deposited by ice until around 14 ka, when Unit C begins.

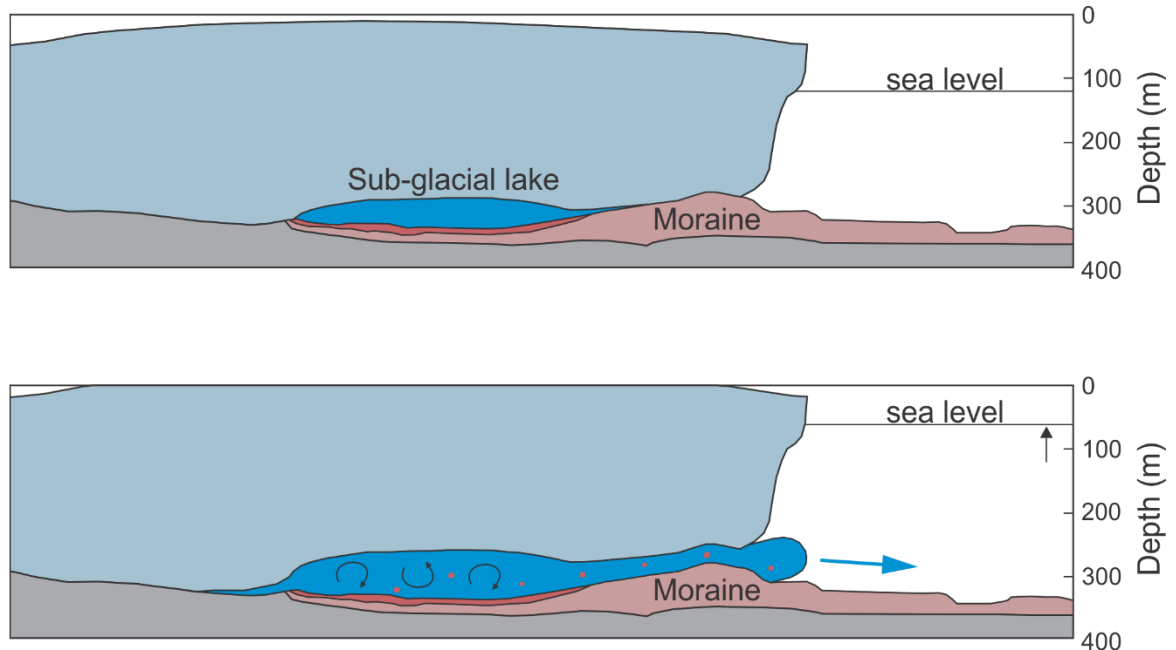


Figure 24. Evacuation of fresh water from sub-glacial lake. When the sea level rises the head of this glacial water forces it out into the ocean, creating turbulence allowing it to carry muds. Modified from Cameron and King (2011).

Unit C has a much higher sedimentation rate than Unit D based on the carbon-14 dates at 451.5-452.5 cm and 763-764 cm. According to Shaw et al. (2006) the Newfoundland ice had largely retreated onto land by 14 ka. This lack of coastal ice is reflected in the lack of IRD and increased sedimentation rate of Unit C. The weak bedding present in the brown muds of Unit C may be due to fluctuations in either source material or current strength. Once the glaciers were on land, broken off ice could no

longer reach the ocean as ice bergs and deposit IRD. The large amount of melting would have allowed for a large amount of muds to be put into the ocean, which currents then carried until eventual deposition on the continental shelf. The  $a^*$  values peaking at  $\sim 2$  in Unit C versus  $\sim 3$  in Unit D reflects a smaller influence from the St. Anthony basin. This decreased influence is likely because by this time the ice was no longer calving through the St. Anthony basin. The reason for the grey mud present at the base of Unit C in some cores, 699-770 cm in core 11, is unknown. The grey muds may have been caused by chemical reduction which occurred some time after deposition.

## **5.6 The role of the Labrador Current**

Units B and A of core 11 allow for the interpretation of the effects of the Labrador Current during the Holocene. These units are correlated with Holocene carbonate sedimentation of Cartwright Saddle Jennings et al. (2015) (Fig. 23). Sediments in Units A and B show a different source than that of Units C and D based on XRF data. Units A and B show an overall higher abundance in Rb and lower abundance in Ti and Zr . Unit B also shows an exceptionally high Ca ppm. The carbonate rich tan mud at the base of Unit B correlates with the carbonate wt% at 11.7 ka of Jennings et al. (2017), which is consistent with the carbon-14 date of 11.2 ka taken above it. This makes this carbonate-rich bed at the base of Unit B the Younger Dryas event. After this event, less detrital carbonate was brought by ocean currents during Unit B leading to the deposition of brown muds. Unlike the deposition of brown muds in Unit C, Unit B was influenced by IRD, showing that ice rafting was occurring during this time. The lack of red muds in Unit B indicates that the ice sheet on Newfoundland was landlocked at this time, so that

any IRD was sourced by the Labrador Current. The olive grey muds at the base of Unit B mark a time where glacial activity was slowed and the sediment source changed to what may contain a higher abundance of organic matter. Shortly before 9.7 ka, another burst of glacial activity occurred, bringing with it carbonate-rich sediment and IRD. This second carbonate-rich sedimentation may be caused by the Gold Cove retreat which occurred at 10.6 ka (Jennings et al. 2017). After this carbonate bed there is another break in glacial activity, allowing for the deposition of olive grey muds. The highest carbonate-rich layer is much longer, 115-274 cm in core 11, is assumed to have resulted from multiple different events. Some of these events include the retreat of the Hudson Strait ice stream (9.2 ka), the Noble Inlet retreat (9.1 ka), and the drainage of the Final Lake Agassiz Flood at 8.3 ka (Levac et al. 2011, Jennings et al. 2017). Unit A began depositing after these major glacial events as the slow deposition of mud from the Labrador Current. The sedimentation rate of this unit is likely much slower due to the decrease in sediment supply from glaciers. The trigger weight core for core 11 is entirely this same olive grey mud seen in Unit A of the piston core.

Unit B of this study matches that of 'Unit B' in Murillo et al. (2015) around Flemish Cap, as both are carbonate-rich units with common IRD. 'Unit B' corresponds to the widespread detrital carbonate carried by the Labrador Current through the Hudson Strait during the early Holocene (Murillo et al 2015). Murillo et al. (2015) determined the lowest carbonate bed of 'Unit B' to correspond to the Younger Dryas, which supports the interpretation of the bottom layer of Unit B in NDT being the Younger Dryas event. Above Unit B of both this study and Murillo et al. (2015) is Unit A, which is described as an olive brown to olive grey mud in Murillo et al. (2015) and is described as an olive grey

mud in this study; both Unit As contain little IRD and have low carbonate content, and are interpreted to have the same origin.

### **5.7 Relative age of the slide**

Cores 1-4 from around the slide block (Fig. 5) may constrain the age of the sliding. It is possible the trench in the sea floor near the failed block where core 3 was taken was formed immediately before the deposition of the upper part of Unit B, as Unit B is short and directly overlies Unit D. The absence of Unit B in core 4 may be due to it being taken from the edge of the decollement surface, penetrating older sediments which were covered by Unit A. The absence of Unit B in core 1 from on top of the slide block (Fig. 13) may be due to winnowing of sediment. On this elevated feature Core 2, was taken from the decollement surface from which the slump block slid. Core 2 has a short Unit C overlying Unit D and then Unit G, unrecognized in other cores (Fig. 14b), so that slump block slid late into the deposition of Unit C, exposing much deeper sediment, which then was buried by the overlying units. This would suggest Unit D in core 2 is different from Unit D that is present in core 11, as it would be much deeper. This is supported by Unit D in core 2 not having the bright red mud seen in core 11 at 852-853 cm. However, this would not explain why the shear strength is high in Unit G and not in Unit D. Therefore, another scenario is the slump occurred during the deposition of Unit D, after the bright red mud was deposited. After the slumping occurred, the top of Unit G would have decompressed, accounting for its slightly lower shear strength. In this second scenario the thin Unit C would have to be due to winnowing of sediments in the water column before they could deposit. In either scenario the slump would have occurred

before the trench, as the two potential unconformities for the slump are both in older units than Unit B. Either of these hypotheses may be oversimplifications of the slumping event and sediment deposition around it.

Another potential scenario is that the age of the slump and trench cannot be determined from the sedimentary record in the cores. If cores 1, 3 and 4 were winnowed when unit B was deposited due to a strong current and core 2 not as much. This may also explain why Unit C is so thin in core 2. This hypothesis of the current being stronger during some of the deposition of Unit B is supported by the beds of sand in core 2, which show that at some point muds were selectively removed by the current.

## **6. Recommended work**

### **6.1 Carbon dating**

For studies on the sedimentary record it would be worth obtaining a carbon-14 date below the bright red mud bed. This would answer when this red mud was deposited, and could help answer if it corresponds to H1.

## **7. Conclusions**

- Shaw and Longva (2017) model of the Notre Dame Trough being formed by the erosion of Pleistocene sediments by glaciotectonism is largely correct.
- Before 14 ka the Notre Dame Trough received sediment glacially eroded from St Anthony Basin.
- The Notre Dame Trough has experienced a similar Holocene sedimentation history to that of Flemish Cap and Cartwright Saddle.
- The Notre Dame Trough had little input from the Labrador current for some time before 14 ka.

- The age of slumping event can not be accurately determined with available data, but likely occurred after the glaciotectionism occurred.

## References

- Cameron, D. M. C., & King, L. E. (2011). Possible flood events in large shelf crossing troughs on the Southeast Canadian Margin. Geological Survey of Canada.
- Campbell, D. C. (2005). Major Quaternary mass-transport deposits in southern Orphan Basin, offshore Newfoundland and Labrador. Geological Survey of Canada.
- Jennings, A., Andrews, J., Pearce, C., Wilson, L., & Ólfasdóttir, S. (2015). Detrital carbonate peaks on the Labrador shelf, a 13–7ka template for freshwater forcing from the Hudson Strait outlet of the Laurentide Ice Sheet into the subpolar gyre. *Quaternary Science Reviews*, 107, 62-80.
- Keen, M. J., & Williams, G. L. (1990). *Geology of the continental margin of eastern Canada (Vol. 2)*. Ottawa: Geological Survey of Canada.
- Lazier, J. R. N., & Wright, D. G. (1993). Annual velocity variations in the Labrador Current. *Journal of Physical Oceanography*, 23(4), 659-678.
- Levac, E., Lewis, C. F. M., & Miller, A. A. L. (2011). The Impact of the Final Lake Agassiz Flood Recorded in Northeast Newfoundland and Northern Scotian Shelves Based on Century-Scale Palynological Data. *Abrupt Climate Change: Mechanisms, Patterns, and Impacts*, 139-159.
- Li, G., & Piper, D. J.W. (2015). The influence of meltwater on the Labrador Current in Heinrich event 1 and the Younger Dryas. *Quaternary Science Reviews*, 107, 129-137.
- Piper, D. J.W. (1988). DNAG# 3. Glaciomarine sedimentation on the continental slope off eastern Canada. *Geoscience Canada*, 15(1).

- Rashid, H., Piper, D. J.W., Lazar, K. B., McDonald, K., & Saint-Ange, F. (2017). The Holocene Labrador Current: Changing linkages to atmospheric and oceanographic forcing factors. *Paleoceanography*, 32(5), 498-510.
- Reimer, P. J., Bard, E., Bayliss, A., Beck, J. W., Blackwell, P. G., Ramsey, C. B., ... & Grootes, P. M. (2013). IntCal13 and Marine13 radiocarbon age calibration curves 0–50,000 years cal BP. *Radiocarbon*, 55(4), 1869-1887.
- Shaw, J., & Longva, O. (2017). Glacial geomorphology of the Northeast Newfoundland Shelf: ice-stream switching and widespread glaciotectonics. *Boreas*, 46(4), 622-641.
- Shaw, J., Piper, D. J.W., Skulski, T., Lamplugh, M. J., Craft, A., & Roy, A. (2011). New evidence for widespread mass transport on the Northeast Newfoundland Shelf revealed by Olex single-beam echo sounding. *Geo-Marine Letters*, 32(1), 5-15.
- Shaw, J., Piper, D. J. W., Fader, G. B. J., King, E. L., Todd, B. J., Bell, T., ... & Liverman, D. G. E. (2006). A conceptual model of the deglaciation of Atlantic Canada. *Quaternary Science Reviews*, 25(17-18), 2059-2081.
- Stuiver, M., Reimer, P.J., 1993. Extended 14C database and revised CALIB radiocarbon calibration program. *Radiocarbon*, 35, 215-230.
- Tripsanas, E. K., & Piper, D. J.W. (2008). Late Quaternary stratigraphy and sedimentology of Orphan Basin: implications for meltwater dispersal in the southern Labrador Sea. *Palaeogeography, Palaeoclimatology, Palaeoecology*, 260(3-4), 521-539.
- Zhang, Y., Pe-Piper, G., & Piper, D. J.W. (2014). Sediment geochemistry as a provenance indicator: unravelling the cryptic signatures of polycyclic sources, climate change, tectonism and volcanism. *Sedimentology*, 61(2), 383-410.

## **Web references**

Marine charting and navigation. (November 2017). Retrieved March 16, 2018, from [http://www.olex.no/index\\_e.html](http://www.olex.no/index_e.html)

Natural Resources Canada, Earth Sciences Sector, & Geoscience Branch. (2017, July 04). The Expedition Database. Retrieved March 16, 2018, from [http://ed.gdr.nrcan.gc.ca/index\\_e.php](http://ed.gdr.nrcan.gc.ca/index_e.php)